CHALMERS

# Synchronization processes and synchronizer mechanisms in manual transmissions

## Modelling and simulation of synchronization processes

*Master's Thesis in the International Master Programme in Applied Mechanics*


ANA PASTOR BEDMAR

Department of Applied Mechanics
*Division of Dynamics*
CHALMERS UNIVERSITY OF TECHNOLOGY
Göteborg, Sweden 2013


Master's thesis 2013:20

MASTER'S THESIS IN THE INTERNATIONAL MASTER PROGRAMME IN APPLIED MECHANICS

# Synchronization processes and synchronizer mechanisms in manual transmissions

*Modelling and simulation of synchronization processes*

ANA PASTOR BEDMAR

Department of Applied Mechanics
*Division of Dynamics*
CHALMERS UNIVERSITY OF TECHNOLOGY
Göteborg, Sweden 2013

Synchronization processes and synchronizer mechanisms in manual transmissions
*Modelling and simulation of synchronization processes*
ANA PASTOR BEDMAR



Master's thesis 2013:20
ISSN 1652-8557
Department of Applied Mechanics
Division of Dynamics
Chalmers University of Technology
SE-412 96 Göteborg
Sweden
Telephone: +46 (0)31-772 1000

Cover:
A synchronizer

Chalmers Reproservice
Göteborg, Sweden 2013

Synchronization processes and synchronizer mechanisms in manual transmissions
*Modelling and simulation of synchronization processes*
Master's thesis in the International Master Programme in Applied Mechanics
ANA PASTOR BEDMAR
Department of Applied Mechanics
Division of Dynamics
Chalmers University of Technology

## Abstract

The transmission system is one of the main parts that determines the behavior, power and fuel economy of a vehicle. Transmission performance is usually related to gear efficiency, gear noise and gear shift comfort during gear change.

Synchronizer mechanisms allow gear changing in a smooth way, noiseless and without vibrations, both for the durability of the transmission and the comfort for the users. As a consequence, it is aimed an improvement of the dynamic shift quality, by reducing shifting time and effort, especially in heavy truck applications.

This Master's Thesis project deals with a study of the synchronization processes in manual transmission gearboxes with focus on commercial vehicles. A description of the different types of synchronizers is given, followed by its components and how they interact with each other in order to complete the gear changing process namely the synchronization process. Then, quality factors are indentified and their effect on the performance and thus synchronizer efficiency.

In this project a model of the manual transmission synchronizer is developed. It is divided into eight different phases corresponding to different events in the process. Only the first three phases have been implemented in Matlab and simulated with different values of some design parameters in order to analyze the reponse. The results show a good qualitative agreement with the literature.

Keywords: Synchronization processes, Synchronizers, Manual transmissions, Commercial vehicles

# Preface

This project has been carried out during the Spring term 2013 in the Applied Mechanics department at the Division of Dynamics at Chalmers University of Technology (Göteborg, Sweden). It has been realized under the supervision of the Professor Viktor Berbyuk and Lecturer Håkan Johansson.

# Acknowledgements

I would like to express my special thanks to my supervisors Professor Viktor Berbyuk and Lecturer Håkan Johansson for giving me the opportunity to perform my Master's Thesis at Chalmers and for their dedication, guidance, support and advice in this thesis work.

I also thank to all the friends I have met in Göteborg for their help, encouragement and good mood and making this experience worthwhile.

And finally, but not least, I am deeply indebted to my parents who have supported me throughout my university studies, made possible this exchange experience and believed in me.

# Nomenclature

| | |
|---|---|
| $a$ | Half width of a groove on the conical surface [m] |
| $b$ | Half length of the cone generatrix [m] |
| $c_{oil,i}$ | Oil viscous damping [(kg $\cdot$ m$^2$)/s] |
| $F_{fork}$ | Axial shift force applied on the outer groove of the sleeve [N] |
| $F_{spring}$ | Reaction force detent spring [N] |
| $J_1$ | Rotating inertia of body 1 [kg $\cdot$ m$^2$] |
| $J_{sr}$ | Rotating inertia of synchro ring [kg $\cdot$ m$^2$] |
| $J_{sl}$ | Rotating inertia of sliding sleeve [kg $\cdot$ m$^2$] |
| $J_{sd}$ | Rotating inertia of strut detent [kg $\cdot$ m$^2$] |
| $J_5$ | Rotating inertia of body 5 [kg$\cdot$ m$^2$] |
| $k_{spring}$ | Spring rate [N/m] |
| $m_{sr}$ | Mass of synchro ring [kg] |
| $m_{sl}$ | Mass of sliding sleeve [kg] |
| $m_{sd}$ | Mass of strut detent [kg] |
| $N_{sl}$ | Normal force, sleeve – strut detent [N] |
| $N_{sr}$ | Normal force, sleeve – synchro ring [N] |
| $N_{sd}$ | Normal force, strut detent – synchro ring [N] |
| $N_h$ | Normal force, synchro hub – synchro ring [N] |
| $N_c$ | Normal force, cone surfaces [N] |
| $n$ | Number of internal circumferential grooves on synchro ring [-] |
| $n_p$ | Number of plunges [-] |
| $R_{sl}$ | Mean effective radius on interlock gearing [m] |
| $R_c$ | Mean cone radius [m] |
| $T_S$ | Synchronization torque [Nm] |
| $T_{Di}$ | Drag torque (depending on the rotational speed) [Nm] |
| $T_I$ | Index torque [Nm] |
| $T_C$ | Frictional torque on cone surfaces [Nm] |
| $x_{sr}$ | Axial displacement, synchro ring [m] |
| $x_{sl}$ | Axial displacement, sleeve [m] |
| $x_{sd}$ | Axial displacement, strut detent [m] |
| $\dot{x}_{sr}$ | Axial velocity, synchro ring [m/s] |
| $\dot{x}_{sl}$ | Axial velocity, sleeve [m/s] |
| $\dot{x}_{sd}$ | Axial velocity, strut detent [m/s] |
| $\ddot{x}_{sr}$ | Axial acceleration, synchro ring [m/s$^2$] |
| $\ddot{x}_{sl}$ | Axial acceleration, sleeve [m/s$^2$] |
| $\ddot{x}_{sd}$ | Axial acceleration, strut detent [m/s$^2$] |
| $y_{sd}$ | Radial displacement, strut detent [m] |
| $\dot{y}_{sd}$ | Radial velocity, strut detent [m/s] |
| $\ddot{y}_{sd}$ | Radial acceleration, strut detent [m/s$^2$] |
| $\alpha_c$ | Cone angle [°] |
| $\beta$ | Chamfer angle [°] |
| $\omega_g$ | Angular velocity, body 1 [rad/s] |
| $\omega_{sr}$ | Angular velocity, synchro ring [rad/s] |
| $\omega_{sl}$ | Angular velocity, sleeve [rad/s] |
| $\omega_{sd}$ | Angular velocity, strut detent [rad/s] |
| $\omega_{out}$ | Angular velocity, body 5 [rad/s] |
| $\dot{\omega}_g$ | Angular acceleration, body 1 [rad/s$^2$] |

| | |
|---|---|
| $\dot{\omega}_{sr}$ | Angular acceleration, synchro ring [rad/s$^2$] |
| $\dot{\omega}_{sl}$ | Angular acceleration, sleeve [rad/s$^2$] |
| $\dot{\omega}_{sd}$ | Angular acceleration, strut detent [rad/s$^2$] |
| $\dot{\omega}_{out}$ | Angular acceleration, body 5 [rad/s$^2$] |
| $\phi$ | Sleeve detent ramp angle [°] |
| $\chi$ | Second chamfer angle [°] |
| $\mu_{sl}$ | Coefficient of friction, strut detent – sleeve [-] |
| $\mu_s$ | Coefficient of friction, sleeve – synchro ring [-] |
| $\mu_c$ | Coefficient of friction, cone surfaces [-] |

# Contents

# 1 Introduction

## 1.1 Project background

The transmission system is one of the main parts that determines the behavior, power and fuel economy of a vehicle. Transmission performance is usually related to gear efficiency, gear noise and gear shift comfort during gear change (Sandooja, 2012).

Synchronizer mechanisms were developed in the 1920s to allow gear changing in a smooth way, noiseless and without vibrations both for the durability of the transmission and the comfort for the users. What is sought is dynamic shift quality, by means of reduced shifting time and shift effort, especially in heavy truck applications since the torques in the drive train are larger.

Several technical papers and patents are focused on the design and performance of this component. However, all these publications have different contributions to the main topic. Some give a description of the main aspects of the changing mechanism and the working principle and introduce basic calculation of the principal parameters (Yuming, 2011), (Vettorazzo et al., 2006), (Razzacki, 2004). Others offer a description of new designs for synchronizers and their single components in order to amplify their capacity in terms of reducing the synchronization time or the effort at gear shift lever, especially in the lower speeds where the gear reduction ratio is larger (Sandooja, 2012), (Spreckels, 2012). In addition, to reduce the double bump phenomenon and improve the shift feeling perceived by the driver (Sharma and Salva, 2012).

Previous researchers have dealt with several mathematical and computational models of synchronization processes and have validated them with experimental data from test rigs (Lovas et al., 2006), (Liu and Tseng, 2007), (Kelly and Kent, 2000), (Hoshino, 1999). However, as said in reference Häggström, D. and Nordlander, M. (2011), they do not offer much information about the performance of the simulations. Additionally, as it is known that drag torque contributes significantly to the engagement of synchronizers in transmissions and can cause the mechanism to fail, some publications are studies of different models of the affecting drag (Berglund, 2012). Other authors go deeper in modelling and direct their attention to the effect of the friction and the consideration of the different stages of lubrication during the process (Lovas et al., 2006), (Lovas, 2004), (Paffoni et al., 2000), (Paffoni et al., 1995).

Nevertheless, they all agreed that '*Recognized problems exist, such as second bump, gear-changing noise, or impossible gear changing, the reasons for which are still unknown*' (Lovas et al., 2006).

## 1.2 Problem statement

The purpose of this thesis work is to acquire a better understanding of the synchronization process and synchronizers with focus on heavy truck manual transmissions. It is aimed to identify the quality factors and the problems related to the process.

In addition, it is intended to develop mathematical and computational models that allow to analyze different responses of synchronizer mechanisms as a function of both design parameters and initial conditions in order to improve the synchronization processes.

## 1.3 Limitations

On the one hand, since synchronizer design is usually a proprietary information, exact dimensions are hard to obtain. Therefore, input parameters (design parameters and initial and end conditions) used in the simulations are not real values, but are assumptions according to the literature review. Consequently, the specific numerical values obtained are not as important or relevant as the general behavior of the model and the main characteristics of the plots.

On the other hand, due to lack of time, it has only been modelled the first three phases of the process. However, it is given some preliminary equations for the rest of the stages that could be added to the mathematical model. Besides, the loosening of the ring due to thermal expansion is hard to include in the model, so for a first approach this effect is not considered.

## 1.4 Thesis outline

This report has been divided into the following chapters:

- Chapter 2 presents an overview of the theoretical part of the synchronizers and the synchronization processes, and determines the important parameters related.
- Chapter 3 gives a description of the different steps followed and the assumptions made in order to obtain the equations of motion of the different components.
- Chapter 4 deals with the implementation of the equations into the software to simulate the synchronization process. In addition, it is studied the effect of the variation of the cone angle, the mean cone radius, the number of internal grooves in synchro ring, the axial load applied to the sleeve and the spring stiffness to the process and the synchronization time.
- Chapter 5 gives the conclusions of this project and some suggestions for further work.

# 2 Theory and Literature Review

## 2.1 Transmission systems in commercial vehicles

Transmission systems can be divided into three different types (Hedman, 2011):

- Manual transmissions, MT:
  - Constant mesh transmission (unsynchronized), CMT (commonly used in North American trucks)
  - Synchronized manual transmission, SMT
- Automatic Transmission (stepped), AT:
  - Automatic planetary transmission, APT
  - Dual-Clutch Transmission, DCT
  - Automatic Mechanically engaged Transmission, AMT
- Continuously Variable Transmission, CVT:
  - Eletro-Mechanical Transmission, EMT

For manual transmissions in commercial vehicles the most common shifting patterns are (Lechner and Naunheimer, 1999):

- Range: They are designed so that the ratio of a particular gear is derived from the individual ratios of two gear pairs. The high-low gear shift split allows the reuse of the same gear shift positions for gears in low and high mode. It is always speed reducing.
- Splitter: This unit can be speed-reducing or speed-increasing with the high-low division. The gears are split into two so that each position is used for two gears.
- Range-splitter: is a combination of the previous types.

Manual Transmissions, Dual Clutch Transmissions and Automatic Mechanically engaged Transmissions use synchronizers to perform the gear changing process. However, the mechanisms used for each type are not the same.

Shift systems in MTs consist of an external shifting mechanism that connects the driver with the gearbox and an internal shifting that transmit the shifting force to the respective synchronizing mechanism and synchronizer. In contrast, in AMTs and DCTs there is no direct connection between the shift lever and the synchronizer. Instead, the shifting force is directed to the internal shifting mechanism electromechanically or hydraulically (Back, O.).

### 2.1.1 Manual transmission in commercial vehicles

Multi-speed transmissions are designed so that the running gears of the individual speeds, even if they are not involved in the power transmission, are constantly engaged. While a gear is fixedly connected to the countershaft, the associated idler wheel can rotate freely on the main shaft (Spreckels, 2001). When a specific speed is needed the free wheel has to be fixed to the shaft. At this moment is when the synchronization processes and synchronizers act. They are positioned between two different speeds hence the synchronizer system is double: apart from the idler position they can choose between two gears.

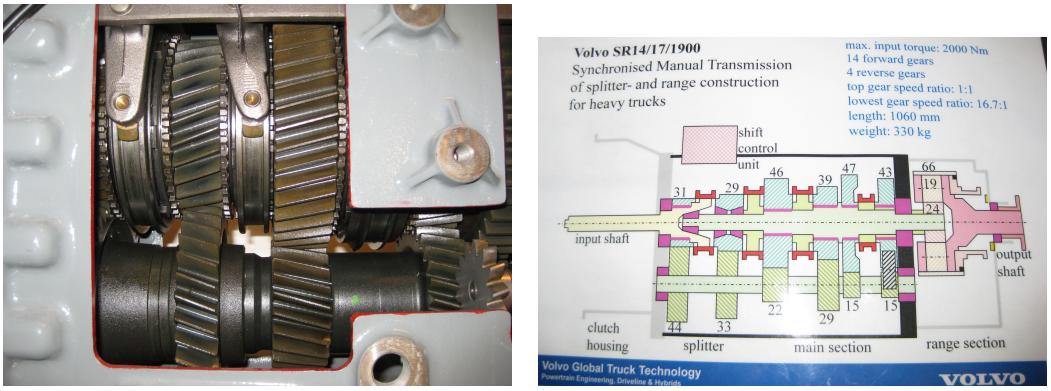


Figure 2.1: *Manual transmission of a commercial vehicle (Volvo SR14/17/1900 gearbox on display at the Department of Applied Mechanics at Chalmers University of Technology, Göteborg, Sweden).*

## 2.2 Synchronization processes theory

Synchronization processes are used in order to get a smooth gear shift and a good shift feel, by reducing the time of synchronization inside the gearbox and the load required at the driver's hand. They prevent transmission gears from shocking, reduce noise and gear wearing and make the driver feel comfortable inside the cabin.

The objective of the synchronization is to reduce to zero the angular speed difference between the rotating shaft and the gear wheel. The principle used is generating a friction torque with a friction contact between conical surfaces before the gear is engaged through a positive locking for torque transmission (Spreckels, 2012).

### 2.2.1 Synchronizer types and components

There are different types of synchronizers designed for gears in parallel shafts; the most common are listed here:

- Pin-type (also known as Clark type).

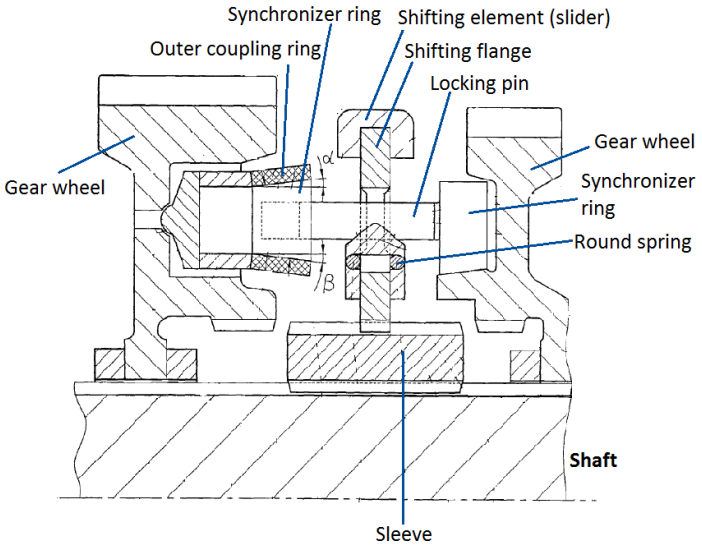


Figure 2.2: *Pin-type synchronizer (U.S. Patent No. 7,431,137 B2).*

- Baulkring-type: this typically used in manual transmissions are either of the strut or the strutless types.

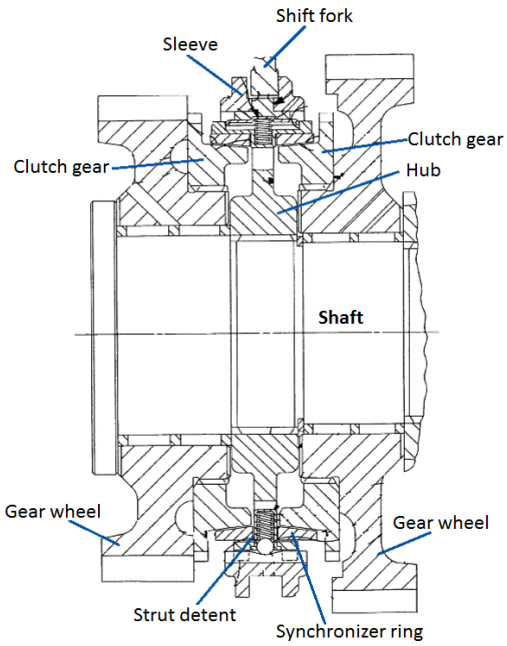


Figure 2.3: *Baulkring-type synchronizer (U.S. Patent No. 7,131,521 B2).*

- Lever-type: the lever is provided in the inner circumference of the sleeve and arranged between the hub and the synchronizing ring. As the sleeve is sliding towards the engaging position the lever presses the synchronizer ring towards the gear by the principle of leverage (U.S. Patent No. 8,020,682 B2).

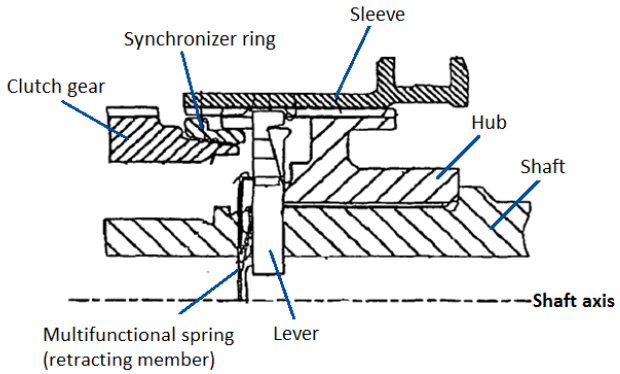


Figure 2.4: *Lever-type synchronizer (U.S. Patent No. 8,020,682 B2).*

Besides, there are other devices adapted to planetary gears for the supplementary gearbox used to double the number of possible gear ratios (Swedish Patent WO 01/55620), see Figure 2.5.

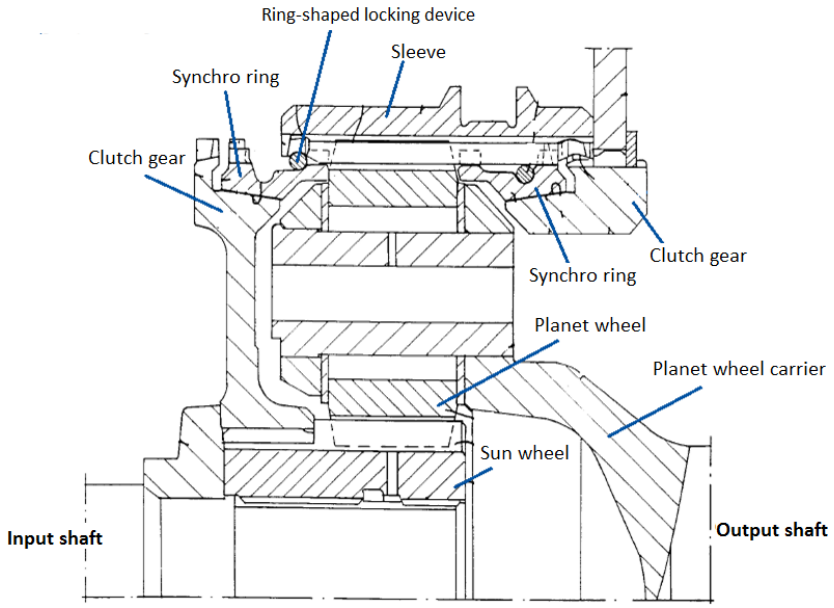


Figure 2.5: *Synchronizer for planetary gears (Swedish Patent WO 01/55620).*

It is known that shift effort increases with vehicle size and weight and that this force may be reduced by the use of synchronizers of the self-energizing type. Therefore, the self-energizing types are especially important for trucks, particularly for heavy duty trucks. Self-energizing means a synchronizer mechanism which includes ramps or boost surfaces in order to increase the engaging force of the friction surfaces by providing an additive axial force proportional to the force applied by the driver to the sleeve (U.S. Patents 5,544,727 and 5,738,194).

Considering a baulkring-type synchronizer with one conical surface clutch as reference, the synchronizer assembly includes (Sandooja, 2012):

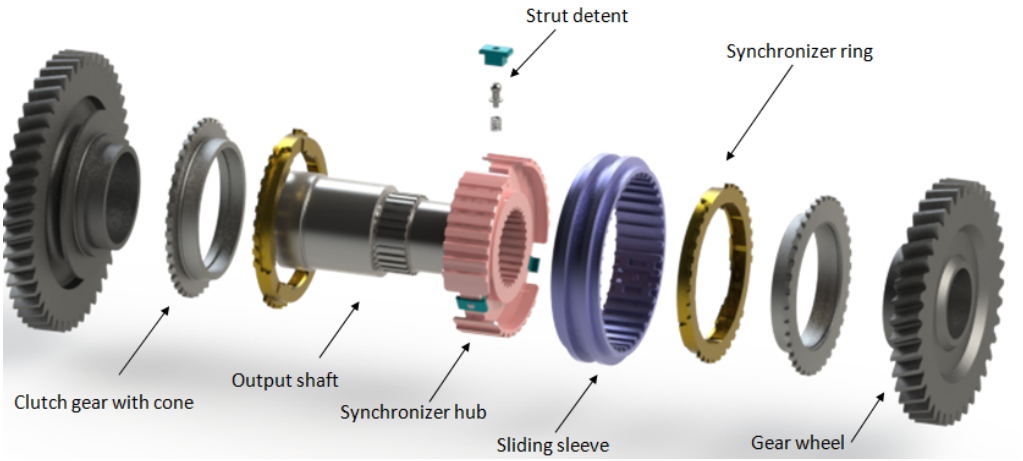


Figure 2.6: *Exploded view of a single-cone synchronizer.*

- **Synchronizer hub**: is rigidly connected by a spline to the rotating shaft (input or output shaft).
- **Sliding sleeve / Gear shift sleeve / Synchronizer sleeve / Coupling sleeve**: has a groove on the outer periphery for the gear shift fork. Includes internal splines that are in constant mesh with the synchro hub external splines, so it is only axially movable from a neutral position to an engaged position.

Both parts and the main shaft work as a single unit hence they move at the same angular speed.

- **Synchronizer ring / Blocking ring / Balk ring / Friction ring**: The external teeth interlock with the internal teeth of the sliding sleeve. It has a conical surface that is fitted with the conical surface of the clutch body ring. Its purpose is to produce the friction torque needed to synchronize the input and output shafts. The cone surfaces are provided with thread or groove patterns and axial grooves in order to either prevent or break the hydrodynamic oil film and minimize force increase (Lovas et al., 2006),(INA, 2007).
- **Clutch gear with cone**: matches the speed of the gear with the speed of the synchro hub. It is either press fitted or laser welded with the gear wheel. The external teeth with chamfer on both sides of the teeth interlock with the chamfer on the internal teeth of shift sleeve.
- **Gear wheel**: normally is connected to the main shaft by a needle bearing for relative rotation between both components and secured against axial movement relative to the shaft. It can also be mounted on the shaft with a very smooth surface and proper lubrication (hydrodynamic bearing).
- **Strut detent / Centring mechanism / Strut key**: spring loaded ball or roller fixed in a cage. Is arranged on the circumference of the synchronizer body, positioned between the groove in synchro hub and the inner groove in shift sleeve. Therefore can integrally rotate with the synchro hub and is axially movable with the shift sleeve. This component is used for pre-synchronization; it means that generates the load on synchro ring to perform the synchronization process (INA, 2007). In addition, maintains the sliding sleeve in a central position on the hub between both gear wheels and below a limit axial force. Often, the synchronizers are composed by three of these elements arranged at 120°. In the case of large synchronizers, there are four elements arranged at 90°(Lovas, 2004).

In heavy vehicle gearboxes there is often a need to increase the synchronizing torque for a given shift effort or even in order to reduce it, especially when downshifting into low gears due to the larger gear reduction ratio.

Therefore, other existing alternatives are available by increasing the number of friction rings or cone surfaces. The choice is a matter of wear and efficiency. But also cost and design: the use of a multi-cone solution implies higher manufacturing costs and additional components increase the complexity of the mechanism and design. For example, as said in reference (U.S. Patent No. 5,560,461), in order to increase the transmitted power of the synchronizer more friction surfaces could be used. However, these additional components increase the cost of the device. Another method is to increase the diameter or distance from the axial centreline where the frictional force is applied. Unfortunately, increasing the distance also increase the size and weight of the synchronizer.

Furthermore, the synchronizer system employed in transmission systems can also be subjected to other types of modifications: asymmetric teeth, different location of blocker and engagement teeth, double-indexing in single-cone synchronizers, increasing the stroke length of the shift lever or using a pneumatic or hydraulic servo unit (Sandooja, 2012), (Kelly and Kent, 2000), (Swedish Patent WO 97/49934).

### 2.2.2 Synchronization phases

Depending on sources and specific synchronizer designs the number of phases varies, but the working principle is the same. Therefore, the synchronization process, from the neutral position (when there is no power transmission) to full engagement, could be defined with the following eight steps:

1. **First free fly**: The sleeve moves axially from the neutral position without significant mechanical resistance and make the detent face come in contact with the synchro ring face. In this phase the axial velocity is high and the axial force low. See Figure 2.7a for the initial and final position of this phase.
2. **Start of angular velocity synchronization**: The detent force creates a frictional torque that makes the ring rotate within the available space in the recesses of the synchro hub (Sandooja, 2012), the oil film between cone surfaces is removed and the spline chamfers of the synchronization ring and sleeve get the maximum contact area and a high coefficient of friction. See Figure 2.7a (right) and 2.7b for the initial and final position of this phase.
3. **Angular velocity synchronization**: This phase is over when the gear, synchro ring and sleeve have the same angular velocity. Otherwise, the equilibrium of axial and tangential forces applied on the spline chamfers prevents from continuation of the gear changing process. This last effect is known as interdiction (Figure 2.7b).
4. **Turning the synchro ring**: The synchro ring that was previously heated by the dissipated friction energy, loses the heat and becomes stuck on the cone due to the diameter reduction. The displacement of the sleeve turn the synchro ring and the clutch gear while the chamfers remain in contact (Figure 2.7c).
5. **Second free fly**: The sleeve moves forward axially until approaching the spline chamfers of the clutch gear (Figure 2.7d).
6. **Start of the second bump**: As there is an oil film that has to be broken between the chamfer surfaces, an increase of the axial force is required in order to maintain the axial velocity of the sleeve. As the oil is being discharged this axial force suffers a higher increment. This stops when the tangential force component on the chamfers is high enough to turn the synchro ring which was stuck in the cone (Figure 2.7e).
7. **Turning the gear**: The axial force required to turn the gear depends on the relative position of the sleeve splines and gear splines (obtained at the end of the synchronization, phase 3). See Figure 2.7f for the end position of this phase.
8. **Final free fly**: The gear wheel is engaged, see Figure 2.7g.

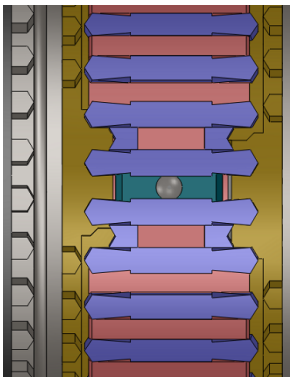

(a) *Initial and final position of First free fly (phase 1).*

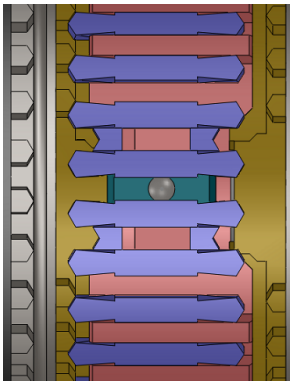

(b) *Spline position during the Angular velocity synchronization (phase 3).*

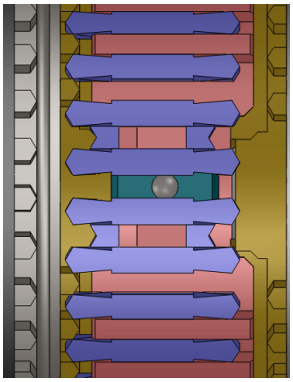

(c) *Final position of Turning the synchro ring (phase 4).*

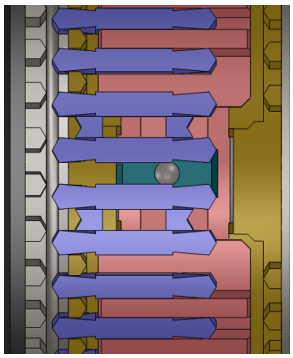

(d) *Second free fly (phase 5).*

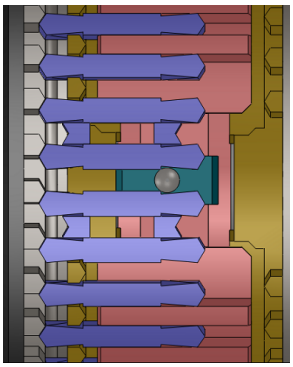

(e) *Spline position during the Start of the second bump (phase 6).*

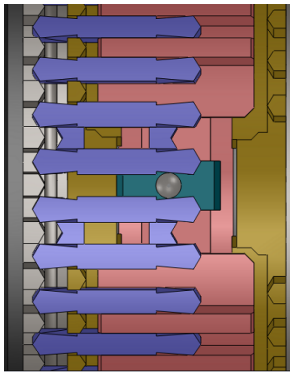

(f) *Final position of Turning the gear (phase 7).*

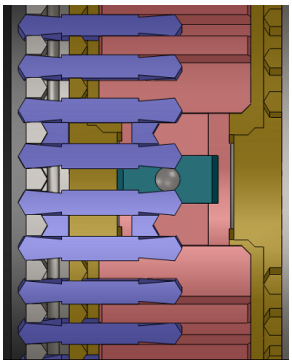

(g) *End position of Final free fly (phase 8).*

Figure 2.7: *Spline position during the synchronization process.*

A detailed description of the working process can be found in (Lovas et al., 2006).

Although the process is the same for upshift and downshift, the changing times are different. During the upshift, the revolution speed of the gear should decrease. As the power losses help, less gear shift time is required. On the contrary, during downshift the synchronized gear is accelerating, but power losses still try to slow it down. Therefore, the changing time is higher (Lovas et al., 2005).

### 2.2.3 Quality factors

From the point of view of the process, the quality factors of the synchronizers are:

**Shift comfort** (major topic in gearbox design and optimization) is related to:

- Shift effort (operating force): is the load the driver has to apply at the shift lever and is the result of a summation of the static shift effort, due to the ramp profile, and the dynamic shift effort, due to the synchronization action (Sharma and Salva, 2012).
- Feel on the gear shift lever caused by the repulsive force acting on the shift lever when the sleeve hits the clutch cone teeth, known as double bump.

**Shifting time**, since the vehicle is free-rolling with zero transmitted torque in the transmission.

The following effects can be considered as problems that appear during the process that influence negatively to the driving feeling.

**Double bump**: are two force peaks that appear during the phases 6 (*Start of the second bump*) and 7 (*Turning the gear*) and exist in a short period of time. After the synchronization phase synchro ring and clutch gear must be turned in order to engage with the sleeve. Therefore, at first, an axial force is needed to separate the synchro ring from the clutch gear cone. This force appears at the end of the phase 6 and has a deterministic part, determined by some design parameters, and a random part, due to the remaining axial force acting on the synchro ring (force applied by the centring mechanism and remain during all the shifting process). Finally, a turning force is required to complete the meshing process. This force depends on the relative position of clutch gear and hub splines, obtained at the end of the synchronization phase hence it is a random variable. Thus, the double bump is the combination of these separating and turning forces applied on the sleeve (Lovas et al., 2005).
However, inertia, elasticity and damping of the gear changing mechanism, the link between the sleeve and the shift lever, can modify these changing forces and thus the driver does not always feel such intense second bump forces (Lovas et al., 2005). Optimization techniques to minimize this phenomenon can be found in (Sharma and Salva, 2012).

**Stick-slip phenomenon**: appears when a mass is placed on a surface and moved there by a combination of stiffness and damping. There are two contact zones where this phenomenon takes place: the sleeve side contact surface and between the tapered surfaces.
This phenomenon is influenced by the normal force and the sliding velocity of the contact surfaces. So that if (Lovas et al., 2006):

- Normal force is low and sliding velocity is high $\rightarrow$ simple sliding.
- Force increases and velocity decreases $\rightarrow$ harmonic oscillations.
- Force is high and velocity is low $\rightarrow$ harmonic oscillations will be interrupted by a linear displacement $\rightarrow$ stick-slip phenomenon.

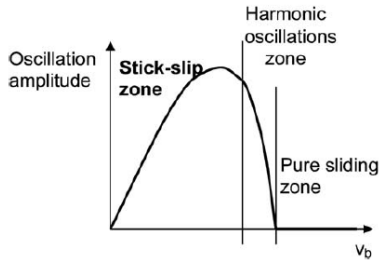


Figure 2.8: *Variation of oscillation amplitude depending on sliding velocity (Lovas et al., 2006).*

This phenomenon is considered to occur either in an axial or in a tangential direction:

- Axial: appears when the sleeve moves axially. However it does not influence the shifting process due to the small values of amplitude oscillations.

- Tangential: occurs when the ring rubs against the clutch gear cone. Although it produces small-amplitude values, it appearance in a sensitive working phase may make it responsible for gear changing noise and cracking.

### 2.2.4 Significant parameters

In this section is given a list of parameters and effects that are present in most synchronization process. In addition, there are the equations that define them.

- **Proximity**: Axial distance from the sleeve tooth pointing to the synchronization ring tooth pointing contact (Razzacki, 2004).

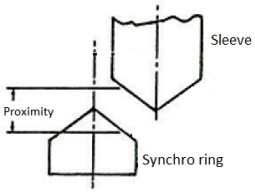


Figure 2.9: *Proximity distance (Häggström and Nordlander, 2011).*

- **Break Through Load (BTL)**: also known as **Push Through Load** is produced by the force applied by the ball of the strut detent to the sleeve in order to traverse the proximity distance. It should start to build as soon as the sleeve moves from the neutral position, due to the contact with the ball, and should stay until there is maximum contact area between the teeth chamfers of the sleeve and the blocking ring (from the phase 1 until the end of phase 2). A reduction of BTL prior to the contact will unload the blocking ring and interrupt the oil wiping action resulting in a lower friction coefficient and, consequently, in gear clash. On the contrary, a BTL continuing beyond the contact point will cause a ring locking and will be required a higher effort to gear shifting.
  The BTL depends on the detent spring rate, strut bump or ball height, coefficient of friction between detent ball and sleeve and ramp angle of the annulus groove in the sleeve (Razzacki, 2004). The mathematical expression of this parameter can be calculated from the Figure 2.10:

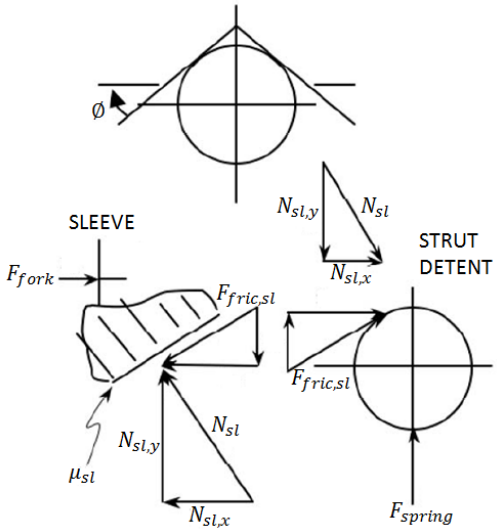


Figure 2.10: *Free body diagram for the BTL (Razzacki, 2004).*

$$F_{fork} = F_{spring}\frac{\mu_{sl}\cos\phi + \sin\phi}{\cos\phi - \mu_{sl}\sin\phi} = F_{spring}\frac{\mu_{sl} + \tan\phi}{1 - \mu_{sl}\tan\phi} \tag{2.1}$$

$$BTL = n_p \cdot F_{fork} \tag{2.2}$$

- **Synchronization torque ($T_S$)**: also known as **cone torque** is due to the friction force generated in the direction of the cone angle between the cone and friction surfaces when the sleeve moves axially to contact with the ring, which pushes axially the clutch cone and drains the lubricant out (Razzacki, 2004). This force can be assisted (upshift) or resisted (downshift) by total system drag (clutch drag, fluid churning and friction losses during upshift or downshift). The synchronization torque can be calculated from the Figure 2.11:

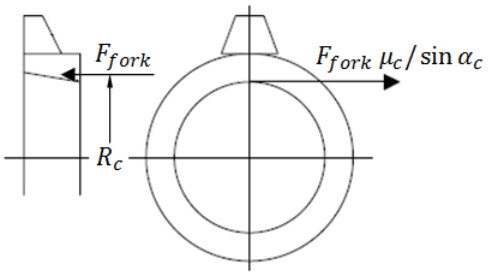


Figure 2.11: *Free body diagram for the friction torque (Razzacki, 2004).*

$$T_S = T_C \pm T_D \tag{2.3}$$

$$T_C = \frac{\mu_c F_{fork} R_c}{\sin\alpha_c} \tag{2.4}$$

This value must be higher than the index torque at every point during the synchronization process to prevent clash or noise (Razzacki and Hottenstein, 2007) and must complete successfully the synchronization process.
The synchronization torque depends on the axial force applied to the sleeve, cone angle, surface coefficient of friction and active cone diameter (Razzacki, 2004).

BTL and cone torque measurements are known in the industry (Razzacki and Hottenstein, 2007).

- **Index torque / Blocking torque ($T_I$)**: is generated due to the friction force in the direction of pointing angle between the two chamfers of synchronizer ring teeth and sliding sleeve teeth. During the synchronization, this torque acts in opposite direction to the synchronizing torque.
  It is a function of the axial force applied to the sleeve, teeth pointing angle, pitch diameter of the blocking ring, surface coefficient of friction between the teeth pointing surfaces of sleeve and blocker ring (Razzacki, 2004). The index torque can be calculated from the following free body diagram (Figure 2.12):

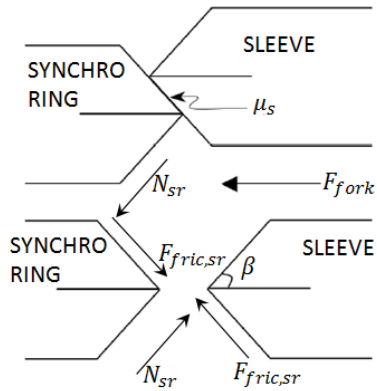


Figure 2.12: *Free body diagram for the index torque (Razzacki, 2004).*

$$T_I = F_{fork} R_{sl} \frac{\cos\beta - \mu_s \sin\beta}{\sin\beta + \mu_s \cos\beta} = F_{fork} R_{sl} \frac{1 - \mu_s \tan\beta}{\tan\beta + \mu_s} \tag{2.5}$$

This value must be higher than total transmission drag in order to satisfy smooth gear shiftability even in cold conditions (Razzacki and Hottenstein, 2007).
Index torque is simply calculated based on geometry and physics and there is no available measurements test procedure in the industry (Razzacki and Hottenstein, 2007).

- **Drag torque ($T_D$)**: are the power losses due to the clutch drag, transmission oil churning and friction of rotating components. Always acts to slow down the speed of rotating components (Sandooja, 2012). According to reference (Razzacki and Hottenstein, 2007) the total system drag can be calculated as follows:

$$T_D = T_{cd} + T_{fc} + T_{frict.} \tag{2.6}$$

Where:
$T_{cd}$: Clutch drag is an uncertain quantity related to wet clutches.
$T_{fc}$: Fluid churning is a function of drive pinion speed and a constant dependent on viscosity, quantity and oil temperature.
$T_{frict.}$: Frictional losses consist of bearing friction, seals, shift and clutch actuation mechanism bending

and deflection and all other friction in the transmission system, as for example the loss due to contact between gear teeth (Berglund, 2012).

- **Shift impulse**: Is the product of the gear shift effort applied to the gear shift knob in Newton (N) and the synchronization time in seconds (s). It is usually used to determine the gear shift performance (Sandooja, 2012).
- **Boost force**: as described in Section 2.2.1, boost force is an additional force generated due to ramp surfaces defined in the hub outer circumference and provides an increase of the shift force without any increase in load on the shift lever (U.S. Patents 5,544,727), (Sandooja, 2012). Note that this design is not implemented in all synchronizers, thus this force is not always present during the process.

From the point of view of the components, the following design parameters primarily affect the synchronization performance and efficiency:

- **Coefficient of friction**: the coefficient of friction on cone-shaped surfaces varies with the thickness of lubricant between the clutch gear/cone (if multiple cone type) and the ring. The coefficient of friction on the cone surfaces increases suddenly, while the sleeve forces the outer ring to move forward the clutch gear/cone for draining lubricant out. It decreases after finishing synchronization, fact that leads the outer ring to slide away from the cone (Liu and Tseng, 2007). Therefore, the friction coefficient is a function of the material, temperature and lubrication (Yuming, 2011).

  Besides, since the synchronization torque is expressed as a function of the coefficient of friction, see equation (2.4), it is preferable to select a material with a high value, such as carbon fiber, molybdenum or brass, in order to increase the synchronizer capacity and, thus reduce the changing time (Yuming, 2011). However, high coefficient of friction produce higher adhesive wear and as a consequence less durability of the synchronizer (Häggström and Nordlander, 2011).
- **Cone angle**: following the same equation (2.4), higher cone torque is exerted with a smaller cone angle. However, in order to avoid self-locking between synchro ring and cone and let the cone leave from contacting the ring after synchronization the following constraint must be satisfied at every time (Liu and Tseng, 2007):

$$\mu_c \leq \tan \alpha_c \tag{2.7}$$

- **Mean cone radius**: following the same equation (2.4), a higher torque will be achieved with a higher radius. However, this also increases the size and weight of the synchronizer. In addition, it has to be taken into account that the available space in the transmission is limited.
- **Number of cones**: increasing the friction surfaces it will be increased the transmitted torque, but also the complexity of the design.
- **Ratio step**: is the distance between each one of the gear ratios in a gearbox. A high step will result in a high relative rotating speed between the input and the output shafts. Therefore the synchronizer will need more mechanical energy to perform its role (Vettorazzo et al., 2006).
- **Roof angle of the sliding sleeve and synchro ring teeth / Pointing angle / Chamfer angle**: determines the way the sleeve and synchro ring are in contact and affect the components of the applied forces. With a lower angle the braking capacity increases since the circumferential force increases. On the contrary, the axial component decreases and could lead to a gear clash due to an inefficient braking.

Moreover, the lower the angle the higher the shift effort will be due to a reduction of the axial force (Vettorazzo et al., 2006).

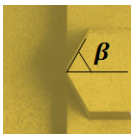


Figure 2.13: *Chamfer angle.*

- **Second chamfer angle on the spline side of the sleeve**: helps to maintain the sleeve in a meshed position, when the sleeve is meshed with the gear splines. A good choice of this angle can reduce the axial force needed to pass beyond the same tangential resistant force (Lovas et al., 2006).


Figure 2.14: *Second chamfer angle.*

- **Width of the synchronizer ring cone surface**: is a function of the materials, lubrication and friction power per unit area. Generally a cone width value is taken:

$$Width = \frac{R_c}{10 \sim 14}$$

  in order to avoid the burn of the synchronizer ring (Yuming, 2011).

- **Boost surface angle / Self-energizing ramp angles**: are defined in the hub outer circumference. On the one hand, it has to be high enough in order to produce the additional force/boost force of magnitude sufficient to increase the synchronizing torque and minimize the synchronization time in response to a given moderate shift effort by the driver. If the value is too great, the ramp will be self-locking rather than self-energizing. This will affect negatively the shift quality or the shift feeling. In addition, it may over stress the synchronizer components, cause over heating, produce rapid wear of the cone clutch and even override driver's movement of the shift lever. On the other hand, this value has to be low enough to produce a controlled additional force (U.S. Patent No. 5,544,727).

- **Performance ratio**: is the ratio of total shift force and the force applied at the shift lever supplied by the driver:

$$PR = \frac{F}{F_d}$$

  Is a function of the boost surface angle (Sandooja, 2012). As this angle increases, the PR also does, but there is a limit to avoid a self-locking condition of the synchronizer ring.

- **Spring rate**: The spring stiffness affects the reaction force of the spring and thus affects the load transmitted to the synchro ring.

In addition, it has to be considered all those design parameters that affect the magnitude of double bump, since is important for the evaluation of gear shift quality (Lovas et al., 2005), (Lovas et al., 2006):

- **Conicity angle error between real synchro ring and clutch gear conicity angles**: this value differs due to machining tolerances and change owing to continuous wear of the conical surfaces. As the synchro ring is far less rigid than the clutch gear, synchronization force produces the deformation of the synchro ring and reduces the conicity angle error to zero. This deformation results in sticking of the synchro ring cone on the clutch gear cone. Therefore, the separation of these components needs the presence of the second bump.

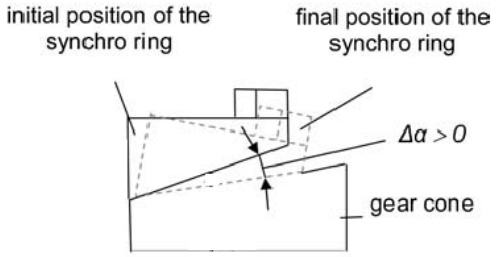


Figure 2.15: *Conicity angle error (Lovas et al., 2006).*

- **Synchro ring material elasticity**: is related to the conicity angle error as referred to before.
- **Synchro ring structural elasticity**: is related to the absorbed heat produced by the friction between conical surfaces. The synchro ring temperature increases and results in thermal expansion, thus an increase of the cone radius. When the heats production stops, at the end of the synchronization, the mean diameter decreases, the surface pressure increases and thus the synchro ring stuck on the gear cone. Again the necessity of the second bump appears.
- **Static friction coefficient between cone shaped surfaces**
- **Friction coefficient on sleeve spline chamfers, gear spline chamfers and synchro ring spline**
- **Sleeve and gear spline chamfer angles**

Moreover, since the stick-slip phenomenon is another problem that appears during the process, its influential parameters have to be taken into account (Lovas et al., 2006):

- Torsional inertia
- Elasticity and damping
- Dynamic and static coefficient of friction between the contact zones
- Critical sliding velocity when harmonic oscillations appear

### 2.2.5 Design defects and errors that affect the performance and efficiency

Synchronization rings are normally secured against a rotation in relation to the synchro hub by the lugs or abutments. However, if they are not well secured, they will have the tendency to undergo uncontrolled movements, such as small radial deflections or tilting movements. These movements express themselves in unpleasant vibrations, causing negative influence on reliability and precision of the process. This contributes to higher shifting times, to faster and increased wear of the friction surface and of the entire of the synchro ring and to shorter the repairing intervals. As a consequence, this affects the driving comfort of the vehicle (U.S.

Patent No. 8,342,307 B2).

Pitch and position error can be produced in splines of the synchro ring, sliding sleeve and synchro hub (Lovas et al., 2005):

- Pitch error: Depending on the relative position of the spline to the spline middle line some pairs can have contact in the chamfer edge, others on the front side chamfer or on the rear side chamfer. Continuation of the shifting process depend on the ratio of these contacts within the spline pairs.

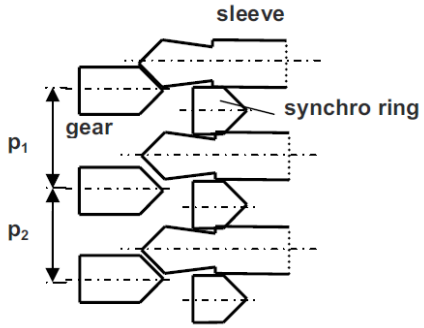


Figure 2.16: *Engagement with pitch error (Lovas et al., 2005).*

- Position error: In this case the contacts are not realized in all spline pairs in the same time. Therefore, teeth slightly in front of the mean spline position come into contact with the teeth of the other component earlier. This makes them have higher load and suffer heavier wear. On the contrary, those teeth behind the mean position are charged during less time.

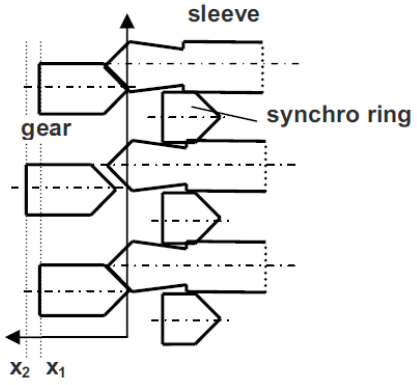


Figure 2.17: *Engagement with position error (Lovas et al., 2005).*

Conicity angle error: the effects are explained in Section 2.2.4.

If the synchro ring is worn and its conical surface is deformed, it does not feel resistance when gear changing and the gear is engaged with a sharp crack. The same happens if the teeth of the synchro ring are worn or deformed (Lovas, 2004).

Impossible change is considered when the gear shifting cannot be performed in a reasonable period of time. Lovas (2004) gives several explanations to this problem:

- Cold gearbox: the viscosity of the oil may be very high hence it can make impossible to break the oil film between the conical surfaces.
- A gearbox overheated: after a long synchronization, the synchro ring can be heated and expand because of the heat dissipation due to friction. Once the synchronization is reached the heat production due to friction disappears, ring cools abruptly and gets stuck in the cone. The position of the synchro ring and clutch gear teeth is not the same, so the interconnection without relative deviation will be more difficult or even impossible.

### 2.2.6 State of art of simulation software and results

MATLAB/Simulink:

- Developed by Ricardo (2000) included the entire selector, transmission, driveline and synchronizer models. The shifting process was divided into five stages with the problems that can arise at each stage of the gearshift process.
- Häggström, D. and Nordlander, M. (2011): Developed a program for calculating heavy truck gearbox synchronization. It was made to support different shift scenarios and different types of gearboxes. It was also considered the values of drag that had been experimentally measured.

ADAMS™:

- Hoshino, H. (1999): Developed a simulation for describing the synchronization mechanism of a transmission for heavy-duty trucks. Divided the process of shifting gears into six events and simulated an upshift. This paper deals with the influences of the shifting speed and friction coefficients. The simulation with three different shifting speeds resulted in different first contact points of the gear spline chamfer which led to different processes of spline meshing. However, although having influence on synchronization mesh between the sleeve and the clutch gear, neither the linkages nor the drivetrain were included.
- Liu, Y-C. and Tseng, C-H. (2007): Developed a simulation model of a strutless double-cone synchronizer when shifting from first to second gear ratio. This paper divides the simulations in two scenarios: synchronized module and meshing module, depending on the position of the sleeve. This was because the previous simulation results, no matter displacement or relative rotational velocity, were the same before finishing engaging with the outer ring, and different after that. On the second scenario, the random mesh process between the sleeve and the clutch gear was divided into four situations, see Figure 2.18. This is due to the different ways of movements depending on the different mesh angles between the sleeve and the clutch gear. Certain mesh angles lead into the forward and backward movements of the sleeve, but the sleeve only moves forward at some mesh angles. The line of demarcation between all these sections would be different if the simulation condition were changed.

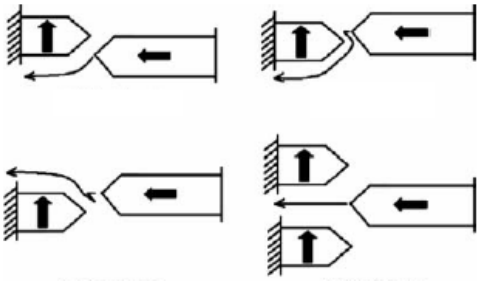

Figure 2.18: *Mesh situations (Liu et al., 2007).*

Shift feeling simulator:

- Developed by Kim et al. (2002): included a model of the external linkage, internal linkage, synchronizer and drivetrain. The synchronizing motion was modelled as eleven steps depending on the relative displacement of the sleeve to the ring spring, outer ring chamfer and gear chamfer. The simulator was able to calculate the sleeve displacement, cone torque, poppet ball torque, sleeve force, shift force and the speed of input and output shaft.

Delphi informatics' environment (Pascal language):

- Numerical simulation developed by Lovas et al. (2006). This simulation included a model of power losses in the car manual gearbox, a heating model of synchro ring, an elastic deformation model of the synchro ring, a model for the start of the second bump, a gear turning model and a model of stick-slip phenomenon. The governing parameters were either the axial velocity or the axial force applied on the sleeve. In addition, it was divided into modules which corresponded to each working phase. Parameters transmitted from one phase to another were the sleeve axial position, synchronized angular velocity and the axial force applied on the sleeve. The occurrence of stick-slip phenomenon was observed in each non-free fly phase. Numerical results showed the variation of the shifting time as a function of angular velocity difference, engaged inertia and changing axial force.

# 3 Mathematical Model

In order to determine the equations of motion for the synchronization process it should be determined the different bodies that the model comprises. This division is not made according each single part of the assembly, but in connection to the movements of them.

In the following Table (3.1) the different bodies are listed and the components forming them. It is also indicated the characteristics of each one.

| **Body** | **Components** | **Type** | **Parameters** | **Degs. of freedom** |
|---|---|---|---|---|
| **1** | Input shaft, gear wheels, counter-shaft, clutch half | Rigid body | $J_1$, $c_{oil,1}$ | $\omega_g$ |
| **2** | Synchro ring 1 (left side) | Rigid body | $J_{sr}$, $m_{sr}$, $c_{oil,2}$ | $x_{sr}$, $\omega_{sr}$ |
| **3** | Sliding sleeve | Rigid body | $J_{sl}$, $m_{sl}$, $c_{oil,3}$ | $x_{sl}$, $\omega_{sl}$ |
| **4** | Strut detent | Rigid body | $J_{sd}$, $m_{sd}$, $k_{spring}$ | $x_{sd}$, $y_{sd}$, $\omega_{sd}$ |
| **5** | Synchro hub, synchro ring 2 (right side), output shaft | Rigid body | $J_5$ | $\omega_{out}$ |
| **6** | Driveline: from the output of the gearbox to the wheels | Elastic body | $J_{drive}$, $k_{drive}$ | |

Table 3.1: *Characteristics of the different bodies.*

## 3.1 Interaction between bodies

Despite the different degrees of freedom stated above, not all are independent and some are equal to the ones corresponding to other bodies either due to the design itself or the process. In addition, for the mathematical model it must be heeded the reaction loads due to the contacts between bodies. For this reason, a study of the interaction between bodies has been made depending on the stages of the process. The following Figure 3.1 illustrates the different contacts that appear throughout the synchronization process.

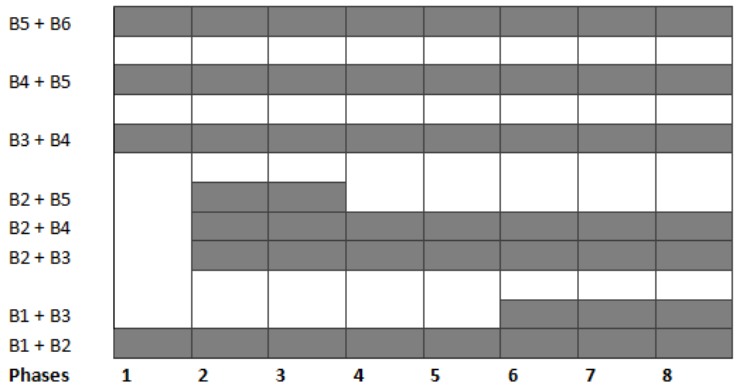


Figure 3.1: *Interaction between bodies throughout the synchronization process.*

**Body 1 – Body 2.** There is a contact during the whole process between the cone surfaces of the clutch gear and the synchro ring, but the magnitudes and the relative movements vary.

The forces that should be considered are:

- Sliding friction force due to the translation of the ring towards the clutch gear ($F_{fric,ct}$).
- Tangential friction force due to the relative rotation between both bodies. This is supposed to be of higher value than the previous one since the relative velocity is higher than the translation one. In addition, it is the responsible of the velocity synchronization by creating the friction torque ($F_{fric,c}$).
- Normal force due to the contact between cone surfaces ($N_c$).

As said before, the interaction depends on the phase of the process. That is, the relative translation last from the first phase to the second one. There is no relative rotation after the synchronization itself since the synchro ring becomes stuck on the cone, and remains until the *Start of the second bump* phase, that has to be separated in order to get a successful gear engagement.

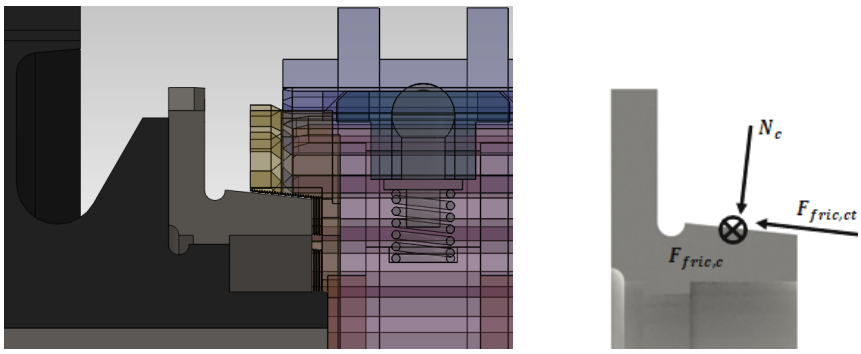


Figure 3.2: *Free body diagram of the clutch gear.*

Figure 3.2 shows the free body diagram of the clutch gear during the phase 2 with the friction and contact loads represented.

**Body 1 – Body 3.** The interaction between these two bodies appears at the end of the process. In particular, it begins with the *Start of the second bump* (phase 6) when approaching the clutch gear and finishes with the *Last free fly* (phase 8), when the gear shifting is completed. The forces that should be considered are:

- Normal force between the clutch gear teeth and the sleeve teeth ($N_g$). It can be decomposed by an axial and a tangential force. The tangential component from the phase 6 helps to separate the synchro ring from the clutch gear and the one corresponding to the phase 7 turns the clutch gear. Both axial and tangential components are responsible of the second bump phenomenon.
- Friction force due to the contact between the clutch gear and the sleeve ($F_{fric,g}$).

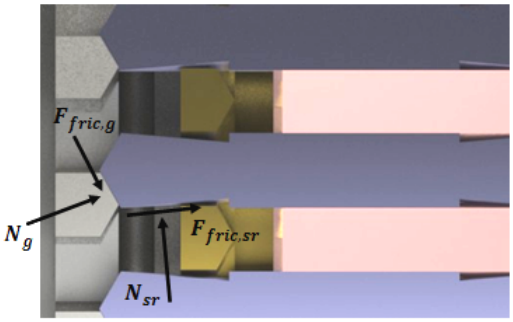


Figure 3.3: *Free body diagram of the contact between the sleeve, sycnchro ring and clutch body gear teeth.*

In Figure 3.3 it can be seen the interaction between body 1 and 3 during phase 6.

It has to be taken into account that the magnitude of these loads depends on the relative position of the sleeve splines and the gear splines obtained at the end of the *Angular velocity synchronization* phase (see Figure 2.18).

**Body 2 – Body 3.** Contact between the splines of the sleeve and the synchro ring. However, it is not always the same. The first interaction appears at the *Start of the angular velocity synchronization* phase between the chamfer surfaces. From the *Second free fly* (phase 5), the contact takes place on the lateral sides of the teeth. Therefore, the loads produced are:

- Normal force ($N_{sr}$) between chamfer surfaces (see Figure 3.4) and lateral surfaces (see Figure 3.3). However, they do not act simultaneously.
- Friction force since there is relative movement of translation in the axial direction ($F_{fric,sr}$).

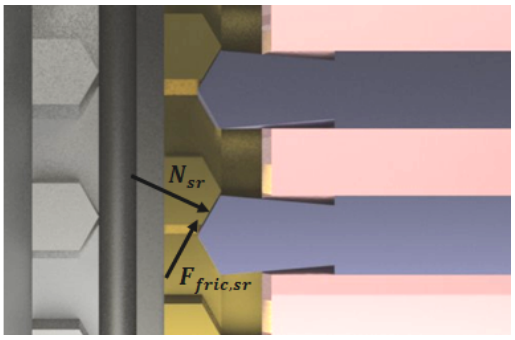


Figure 3.4: *Free body diagram of the contact between the teeth chamfers of sleeve and synchro ring.*

**Body 2 – Body 4.** The contact starts with the activation of the shift lever and the distance between the strut detent and the synchro ring has vanished, just at the beginning of the second stage. The movement of the sleeve gives a displacement of the strut detent that pushes the synchro ring during the whole process. The load that must be heeded is:

- Normal force in the axial direction due to the contact of the surfaces ($N_{sd}$).

In addition, it will be considered the friction force ($F_{fric,sd}$) produced due to the relative rotation of the synchro ring within the available space in the hub while the strut is acting on it, see Figure 3.5. This friction

load will be present at phase 2 and 4. However, the friction on the radial direction due to the compression of the spring is not included.

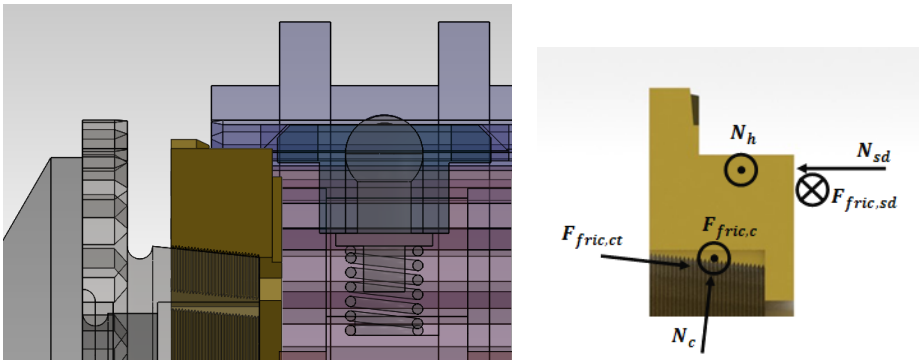


Figure 3.5: *Free body diagram of synchro ring 1.*

**Body 2 – Body 5.** The interaction takes place in the first stages. As soon as there is a torque between the cone surfaces, the synchro ring is able to rotate. Since it can only rotate within the available space in the slots of the synchro hub, the synchro ring lugs immediately come into contact with the synchro hub (see Figure 3.6). The load that has to be considered is:

- Normal force in the tangential direction due to the contact of the bodies ($N_h$).

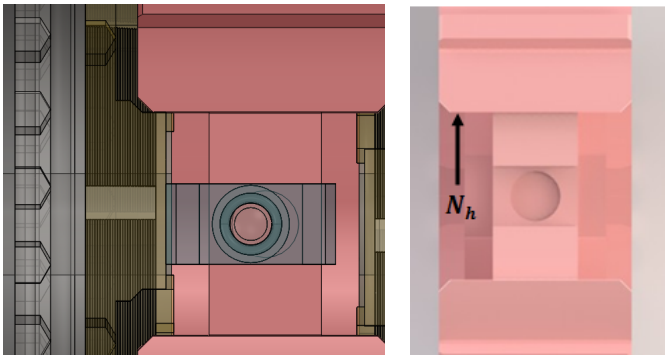


Figure 3.6: *Free body diagram of synchro hub.*

If the synchro hub is designed with boost surfaces, there is another force rising due to this contact. It is called boost force, which axial component assists the load applied by the driver at the shift lever.

**Body 3 – Body 4.** Both components are rotating together. However, when the spring is compressed, there is relative movement of translation between them. Therefore the interaction of the bodies is not always of the same nature.

The loads that should be studied are:

- Normal force, since the bodies are in contact ($N_{sl}$).
- Friction force due to the relative translation ($F_{fric,sl}$).

- Spring load in the radial direction since is compressed all the time ($F_{spring}$). This last force affects the two previous ones mentioned.

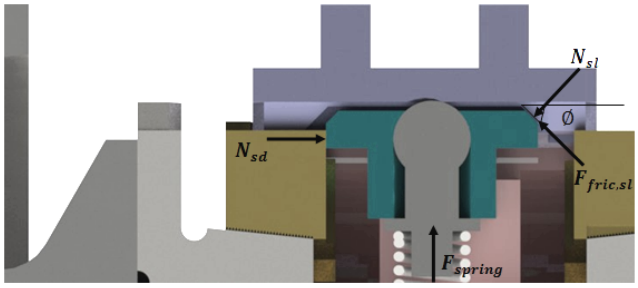


Figure 3.7: *Free body diagram of strut detent.*

**Body 4 – Body 5.** The interaction is constant during the process since they are rotating together. When a relative movement of translation exists, it has to be considered a friction force between the lateral surfaces of the teeth.

**Body 5 – Body 6.** The output shaft is the connection with the body 6 and the interaction is the same during the whole process.

Furthermore, in order to model the movements of the components, the following assumptions have been made:

- Since there is oil between the cone surfaces and teeth, clutch gear and synchro ring are interacting at every time of the process. However, the magnitude of the loads produced is changing depending on the phase.
- Synchro ring 2 (right side) has a limited relative rotation with relation to the synchro hub. It is therefore considered to move following the synchro hub rotation and considered part of the same body with respect to rotation.
- The strut detent assembly (spring, ball or roller and housing) is considered as a single unit hence the equation can be useful for the different existing types of struts.
- The friction forces due to the contact between the teeth of the synchro hub and the sleeve are neglected. On the contrary, the friction forces due to the relative movement between the strut detent face and the synchro ring lug are taken into account since they depend on the axial force applied to the sleeve.
- The gearbox temperature and viscosity of the oil remains constant during the whole process.
- As the synchro ring is considered as a rigid body, its deformation during the process due to thermal expansions and contractions is not taken into account.
- The influence of the conicity angle error between real synchro ring and clutch gear conicity angles is not studied.
- It is not considered neither pitch nor position errors in the model.
- Power losses are considered to be proportional to the angular speed of the different bodies as:

$$T_{Di} = -\text{sign}(\omega_i) \cdot c_{oil,i}\omega_i \tag{3.1}$$

- The process starts at the neutral position and the sleeve is at rest as initial condition.

## 3.2 Equations of motion

In addition to divide the synchronizer into different bodies to study their movement, the process is divided into different stages, as seen in Section 2.2.2. As a consequence, the equations of motion will vary according to the behavior of the components in each phase. In this section the equations of motion are shown. The ones corresponding to the first 3 phases have been introduced in Matlab (see Chapter 4). However, the ones for the next phases are preliminary equations, which mean that for the implementation in Matlab they may need additional constraints and/or assumptions.

Before going deeper to the equations of motion, it has to be taken into account if the model is performing an upshift or a downshift due to some differences on the equations and thus the changing times. According to Back, O., during downshifts, acceleration of the engine-side rotating masses results in performance loss. Conversely, during upshifts the engine-side rotating masses are decelerated and the resulting energy is available as driving power during shifting.

In this project it is considered an upshift. In this case, before the gear change, the target gear is rotating at a higher speed than the output shaft, hence the gear wheel has to be slowed down. Here the clutch drag helps to brake the rotation of this component, acting as an aid torque for the synchronization torque.

- **Phase 1:**
  This phase is considered to end when the strut detent has travelled the axial distance needed to come into contact with the synchro ring. Consequently, this last component does not receive any axial force and thus does not move axially.

  The active degrees of freedom of this stage are: $\omega_g$, $\omega_{sr} = \omega_{sl} = \omega_{sd}$, $x_{sl}$, $x_{sd}$ and $y_{sd}$. According to them, the motion equations are the following:

  Body 1:
  $$J_1 \, \dot{\omega}_g = T_{D1} \tag{3.2}$$

  Body 3:
  $$m_{sl} \, \ddot{x}_{sl} = F_{fork} - N_{sl}(\sin\phi + \mu_{sl}\cos\phi) \tag{3.3}$$
  $$(J_{sr} + J_{sl} + J_{sd} + J_5) \, \dot{\omega}_{sl} = T_{D3} \tag{3.4}$$

  Body 4:
  $$n_p m_{sd} \, \ddot{x}_{sd} = N_{sl}(\sin\phi + \mu_{sl}\cos\phi) \tag{3.5}$$
  $$m_{sd} \, \ddot{y}_{sd} = F_{spring} + \frac{N_{sl}}{n_p}(\mu_{sl}\sin\phi - \cos\phi) \tag{3.6}$$

  In addition, the geometrical constraint that should appear in the system is:

  $$x_{sl} - x_{sd} = \frac{\Delta y_{sd}}{\tan\phi} \tag{3.7}$$

  Here, $y_{sd}$ is the radial position of the strut detent from the axis of rotation to the centre of the detent ball, $x_{sl}$ and $x_{sd}$ are the axial positions of the sleeve and the strut detent, respectively, and have their reference value at the neutral position.

For the spring force, it is considered the deformation due to the bending of the spring when the strut detent is pushed by the sleeve and thus displaced axially. The equation of this load is as follows:

$$F_{spring} = k_{spring} \left( L_{spring,0} - \sqrt{\left(x_{sd}^2 + L_{spring}^2\right)} \right) \tag{3.8}$$

Where $L_{spring}$ is the length of the spring in the vertical direction once mounted and depends on the radial displacement ($y_{sd}$), and $L_{spring,0}$ is the length without compression.

However, depending on the value of the detent spring stiffness and the force applied at the fork, the strut detent moves either axially with the same speed as the sleeve, following it until the strut detent reaches the synchro ring face; or the ball withdraw into its housing and there is a relative translation between both bodies.

On this first phase, it has also been considered the possibility of the non compression of the spring during the axial movement and the system results having a degree of freedom less. Therefore, the new degrees of freedom are: $\omega_g$, $\omega_{sr} = \omega_{sl} = \omega_{sd}$, $x_{sl} = x_{sd}$ and $y_{sd}$ and the equations corresponding to both bodies change, (3.3) and (3.5).

Body 3 and 4: $$(m_{sl} + n_p m_{sd})\ \ddot{x}_{sl} = F_{fork} \tag{3.9}$$

- **Phase 2:**
  During this phase, the axial velocity of the sleeve decreases to zero, and the same for the strut detent and synchro ring. The reason is that on the one hand, both strut and synchro ring have the limitation from the clutch body gear, so there is no more space to move. On the other hand, the teeth chamfers of the sleeve come into contact with the teeth chamfers of the synchro ring.

  The active degrees of freedom considered for this phase are: $\omega_g$, $x_{sr} = x_{sd} = x_{sl}$, $\omega_{sr}$, $\omega_{sd} = \omega_{sl}$ and $y_{sd}$.

  Note that the angular velocities of the synchro ring and the sleeve are almost the same. However, for a moment there is a relative movement between them when a frictional torque appears between the cone surfaces and the synchro ring rotates within the clearance of the slots of the hub until reaching the face.

  In addition, during this stage the movements to collapse the oil film between the cone surfaces are described by hydrodynamic equations. For this case is used the viscous stage that considers the presence of a complete oil film. For more details see references (Paffoni et al., 1995), (Paffoni et al., 2000) and (Lovas, 2004).

  The system of equations of this phase is:

  Body 1: $$J_1\ \dot{\omega}_g = T_c + T_{D1} = K_{CC} 4\pi\mu \dot{x}_{sr}\ R_c^3\ \omega_{sr} \frac{b}{h} \left(1 - \frac{\omega_g}{\omega_{sr}}\right) + T_{D1} \tag{3.10}$$

  $$K_{CC} = 1 + (1-n)\frac{a}{b_i} \tag{3.11}$$

  As $\omega_g > \omega_{sr}$ during an upshift, the frictional torque has a negative value in order to brake the rotation of the gear.

Body 2:
$$(m_{sr} + m_{sl} + n_p m_{sd})\ \ddot{x}_{sr} = F_{fork} - N_{c,ax}\ \left(1 + \mu_c\ \frac{\cos\alpha_c}{\sin\alpha_c}\right) \tag{3.12}$$

$$N_{c,ax} = \begin{cases} 0 & \text{if } h_1 < h \leq h_0 \\ K_{NC} 16\pi\mu\dot{x}_{sr} \sin^2\alpha_c\ R_c \left(\frac{b}{h}\right)^3 & \text{if } h_{min} \leq h \leq h_1 \end{cases} \tag{3.13}$$

$$K_{NC} = \frac{1}{n^2}\ \left[1 + (1-n)\frac{a}{b_i}\right]^3 \tag{3.14}$$

$$b_i = b - \frac{n}{2}a \tag{3.15}$$

$$h = h_0 - (x_{sr} - x_{sr0})\sin\alpha_c \tag{3.16}$$

$$J_{sr}\ \dot{\omega}_{sr} = |T_c| + N_h R_h - N_{sd}\mu_{sd}R_{sd} + T_{D2} \tag{3.17}$$

Where:
$h_1$: is the initial normal distance between the conical surfaces at the beginning of the oil film compression.
$h_{min}$: is considered the closest normal distance between the cone surfaces and takes into account the surface roughness (Lovas, 2004).
$K_{CC}$ and $K_{NC}$: are form factors introduced by the circumferential grooves on the inner surface of the synhcro ring. According to reference (Paffoni et al., 1997), the effect of the axial load and the transmitted torque diminishes very rapidly as the number of grooves increases.
$R_h$: is the radius of contact between synchro hub and synchro ring.
$R_{sd}$: is the radius of contact between synchro ring and strut detent.
$n$: is the number of the circumferential grooves.

The equation (3.12) represents that the three bodies move together, but this is not always the case. If the spring is compressed there is a relative movement between strut detent and sleeve, both axial and radial. Therefore, considering this situation the equations of motion would be:

Body 2 and 4: $(m_{sr} + n_p m_{sd})\ \ddot{x}_{sr} = N_{sl}\ (\sin\phi + \mu_{sl}\cos\phi) - N_{c,ax}\ \left(1 + \mu_c\ \frac{\cos\alpha_c}{\sin\alpha_c}\right)$ (3.18)

Body 3:
$$m_{sl}\ \ddot{x}_{sl} = F_{fork} - N_{sl}\ (\sin\phi + \mu_{sl}\cos\phi) \tag{3.19}$$

The geometrical constraint corresponding to the Equation (3.7) should also appear.

The rest of the equations describing the movements are:

Body 3 and 4:
$$(J_{sl} + J_{sd} + J_5)\ \dot{\omega}_{sl} = N_{sd}\mu_{sd}R_{sd} - N_h R_h + T_{D3} \tag{3.20}$$

Body 4:
$$m_{sd}\ \ddot{y}_{sd} = F_{spring} + \frac{N_{sl}}{n_p}\ (\mu_{sl}\sin\phi - \cos\phi) \tag{3.21}$$

Nevertheless, if it is not considered the relative rotation between the syncro ring and the hub, the equations (3.17) and (3.20) could be replaced by the following formula:

$$(J_{sr} + J_{sl} + J_{sd} + J_5)\ \dot{\omega}_{sr} = |T_c| + T_{D2} \tag{3.22}$$

- **Phase 3:**
  During phase 3, the chamfer teeth of the synchro ring and the sleeve are in contact and do not change the position until the synchronization is achieved. Therefore, there is no axial movement of any of the bodies and the active degrees of freedom are: $\omega_g$, $\omega_{sr}$ and $\omega_{sl}$.

  Besides, the variations of the angular speeds are also described applying the equations of the mixed lubrication that takes place between the conical surfaces. However, in this case it is assumed that the variation of the coefficient of friction is linear with respect to the Stribeck number. See reference (Lovas, 2004).

  The equations of motions referring to this stage of the process are as follows:

Body 1:
$$J_1\ \dot{\omega}_g = -\frac{\mu_c(t) F_{fork}(t) R_c}{\sin\alpha_c}\ \left(1 + \frac{1}{3}\ \left(\frac{b}{R_c}\right)^2 \sin^2\alpha_c\right) + T_{D1} \tag{3.23}$$

$$\begin{aligned}\mu_c(t) &= \mu_{solid} - \frac{\mu_{solid} - \mu_v}{S_2 - S_1}(S - S_1) \\ &= \mu_{solid} + \frac{\mu_{solid} - \mu_v}{S_2 - S_1} S_1 - \frac{\mu_{solid} - \mu_v}{S_2 - S_1} \cdot \frac{\mu(\omega_g - \omega_{sr}) R_c}{F_{fork}(t)}\ 4\pi R_c b \sin\alpha_c\end{aligned} \tag{3.24}$$

Body 2:
$$\begin{aligned}J_{sr}\ \dot{\omega}_{sr} = \frac{\mu_c(t) F_{fork}(t) R_c}{\sin\alpha_c}\left(1 + \frac{1}{3}\ \left(\frac{b}{R_c}\right)^2 \sin^2\alpha_c\right) - N_h R_h - R_{sl}\ \frac{1 - \mu_s \tan\beta}{\tan\beta + \mu_s} \\ \cdot[F_{fork}(t) - N_{sl}\ (\sin\phi + \mu_{sl}\cos\phi)] + T_{D2}\end{aligned} \tag{3.25}$$

Body 3 and 4:
$$(J_{sl} + J_{sd} + J_5)\ \dot{\omega}_{sl} = R_{sl}\ \frac{1 - \mu_s \tan\beta}{\tan\beta + \mu_s}\ [F_{fork}(t) - N_{sl}\ (\sin\phi + \mu_{sl}\cos\phi)] + N_h R_h + T_{D3} \tag{3.26}$$

Where:
$\mu_c$: is the coefficient of friction that varies with the sliding velocity and the axial load applied to the sleeve. Both parameters vary with the time.
The coefficient of friction is represented by the Stribeck curve and the Stribeck number is described as dimensionless viscosity $S$ (Paffoni et al., 2000):

$$S = \frac{\mu U(t)}{p(t)} \tag{3.27}$$

Here, the average sliding velocity can be expressed as:

$$U(t) = (\omega_g - \omega_{sr}) R_c \tag{3.28}$$

and the average pressure as:

$$p(t) = \frac{F_{fork}(t)}{4\pi R_c b \sin\alpha_c} \tag{3.29}$$

$S_1$: is the Stribeck's number at the end of the mixed friction, see reference (Paffoni et al., 2000).
$S_2$: is the Stribeck's number at the start of the mixed friction, see reference (Paffoni et al., 2000).
$\mu_{solid}$: Limiting value of the coefficient of friction at the end of the mixed stage.

$\mu_v$: Initial value of coefficient of friction at the beginning of the mixed stage.

Nevertheless, a simplification for the equations (3.25) and (3.26) can be made. The sleeve and the synchro ring are locked together due to the chamfer contact and remain in the same position until the end of the synchronization phase. Therefore, one can assume that the angular speeds of these bodies are the same and could be expressed as:

Body 2, 3 and 4:

$$(J_{sr} + J_{sl} + J_{sd} + J_5)\ \dot{\omega}_{sr} = \frac{\mu_c(t) F_{fork}(t) R_c}{\sin\alpha_c}\ \left(1 + \frac{1}{3}\ \left(\frac{b}{R_c}\right)^2 \sin^2\alpha_c\right) + T_{D2} \tag{3.30}$$

- **Phase 4:**
  During this phase the synchro ring and the clutch gear are turned so that the sleeve can engage the synchro ring. This relative rotating movement is done while the sleeve is displacing and the synchro ring and struts remain at the same axial position. Besides, the spring is compressed due to this relative axial movement.
  The active degrees of freedom of this period are: $\omega_g = \omega_{sr}$, $x_{sl}$, $\omega_{sl} = \omega_{sd}$ and $y_{sd}$.

  Body 1 and 2:

$$(J_1 + J_{sr})\ \dot{\omega}_g = F_{fork} R_{sl} \frac{1 - \mu_s \tan\beta}{\tan\beta + \mu_s} - N_{sl} R_{sl} (\sin\phi + \mu_{sl}\cos\phi) \frac{1 - \mu_s \tan\beta}{\tan\beta + \mu_s} - R_{sd} N_{sd} \mu_{sd} + T_{D1} \tag{3.31}$$

  Where if considering $\ddot{x}_{sd} = 0$ :

$$N_{sd} = N_{sl}\ (\sin\phi + \mu_{sl}\cos\phi) \tag{3.32}$$

  The angular acceleration of the synchro ring is related with the axial acceleration of the sleeve, so can be also expressed as:

$$\dot{\omega}_g = \frac{\ddot{x}_{sl}\tan\beta}{R_{sl}} \tag{3.33}$$

Body 3: $$m_{sl}\ \ddot{x}_{sl} = F_{fork} - N_{sl}\ (\sin\phi + \mu_{sl}\cos\phi) - N_{sr}\ (\sin\beta + \mu_s\cos\beta) \tag{3.34}$$

Body 3 and 4: $$(J_{sl} + J_{sd} + J_5)\ \dot{\omega}_{sl} = N_{sr} R_{sl}\ (\cos\beta - \mu_s \sin\beta) - R_{sd} N_{sd} \mu_{sd} + T_{D3} \tag{3.35}$$

Body 4: $$m_{sd}\ \ddot{y}_{sd} = F_{spring} - \frac{N_{sl}}{n_p}\ (\cos\phi - \mu_{sl}\sin\phi) \tag{3.36}$$

- **Phase 5:**
  During phase 5 all the bodies are rotating together and there is only axial movement of the sleeve that is moving forward towards the teeth chamfers of the clutch gear. It is also considered that the spring has been totally compressed and thus the contact with the ramp angle of the inner groove of the sleeve does no longer exist. The contact force henceforth is in the radial direction. Consequently, the active degrees of freedom are: $\omega_g = \omega_{sr} = \omega_{sl} = \omega_{sd}$ and $x_{sl}$.

The equations describing the movements are:

Body 3:
$$m_{sl}\ \ddot{x}_{sl} = F_{fork} - N_{sl}\mu_{sl} - N_{sr}\mu_s \tag{3.37}$$

All bodies:
$$(J_1 + J_{sr} + J_{sl} + J_{sd} + J_5)\ \dot{\omega}_{sl} = T_{D3} \tag{3.38}$$

- **Phase 6:**
  During this phase the synchro ring is supposed to be separated from the clutch gear by increasing the axial force and thus the tangential component of this force. In addition, with the axial displacement of the sleeve an oil film between chamfer surfaces is being compressed, requiring a higher force.
  Considering the active degrees of freedom: $\omega_g$, $\omega_{sr} = \omega_{sl} = \omega_{sd}$ and $x_{sl}$, the equations of motion are the following:

  Body 1:
  $$J_1\ \dot{\omega}_g = N_g R_{sl}\ (\cos\beta - \mu_g \sin\beta) - N_c R_c \mu_c + T_{D1} \tag{3.39}$$

  Body 3:
  $$m_{sl}\ \ddot{x}_{sl} = F_{fork} - N_g\ (\sin\beta + \mu_g \cos\beta) - N_{sr}\ (\mu_s \cos\chi - \sin\chi) - N_{sl}\mu_{sl} \tag{3.40}$$

  Body 2, 3 and 4:
  $$(J_{sr} + J_{sl} + J_{sd} + J_5)\ \dot{\omega}_{sl} = N_g R_{sl}\ (\mu_g \sin\beta - \cos\beta) + N_c R_c \mu_c + T_{D3} \tag{3.41}$$

  Where $N_g$ is the normal contact force between the teeth chamfers of the clutch gear and the sleeve and $\chi$ is the second chamfer angle of the sleeve teeth.

  For more information about the equations of this phase regarding the normal distance between chamfer surfaces and the effect of the oil film see references (Lovas et al., 2006) and (Lovas, 2004).

- **Phase 7:**
  During this phase there is relative rotation between the clutch gear and the sleeve and also axial displacement of this last component. So the active degrees of freedom are: $\omega_g$, $\omega_{sr} = \omega_{sl} = \omega_{sd}$ and $x_{sl}$.

  Body 1:
  $$J_1\ \dot{\omega}_g = R_{sl}\ \left[F_{fork}\ \frac{1 - \mu_g \tan\beta}{\tan\beta + \mu_g} - (N_{sr}\mu_s + N_{sl}\mu_{sl})\ \frac{1 - \mu_g \tan\beta}{\tan\beta + \mu_g}\right] - N_c R_c \mu_c + T_{D1} \tag{3.42}$$

  However, the turning of the clutch gear depends on the relative position between this part and the sleeve obtained at the end of the synchronization phase (see Figure 2.18). Reference Lovas et al. (2005) define a random variable ($\xi$) describing this relative position (see Figure 3.8), which is related to the teeth pitch ($p$) and the angle that would have to rotate ($\varphi_g$) (see equation (3.43)).

$$y = \xi p = \varphi_g R_{sl} \tag{3.43}$$

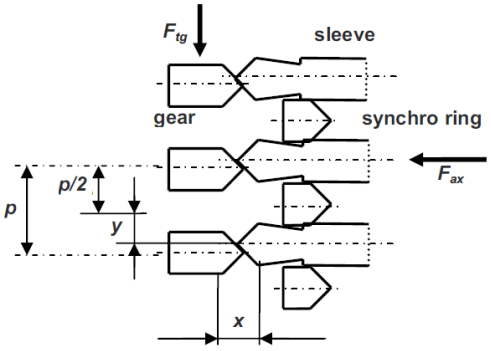


Figure 3.8: *Position of the teeth at the start of the phase 7 (Lovas et al., 2005).*

This variable affects the angular acceleration of the clutch gear:

$$\dot{\omega}_g = \begin{cases} \dfrac{2\varphi_g}{t^2} = \dfrac{2\tan^2\beta\ \dot{x}_{sl}^2}{R_{sl}\xi p} & \text{if } \xi \neq 0 \\ 0 & \text{if } \xi = 0 \end{cases} \tag{3.44}$$

The rest of the equations are:

Body 3: $$m_{sl}\ \ddot{x}_{sl} = F_{fork} - N_{sl}\mu_{sl} - N_{sr}\mu_s - N_g\ (\sin\beta + \mu_g\cos\beta) \tag{3.45}$$

Body 2, 3 and 4:

$$(J_{sr} + J_{sl} + J_{sd} + J_5)\ \dot{\omega}_{sl} = N_g R_{sl}\ (\mu_g\sin\beta - \cos\beta) + N_c R_c \mu_c + T_{D3} \tag{3.46}$$

- **Phase 8:**
  The last phase has axial displacement of the sleeve that is moving towards the engaging position. In addition, all the bodies are rotating at the same speed and the angular velocity is only affected by the power losses.
  The degrees of freedom considered are: $\omega_g = \omega_{sr} = \omega_{sl} = \omega_{sd}$ and $x_{sl}$.
  Therefore, the equations regarding this phase are:

  Body 3: $$m_{sl}\ \ddot{x}_{sl} = F_{fork} - N_g\ (\mu_g\cos\chi - \sin\chi) - N_{sr}\mu_s - N_{sl}\mu_{sl} \tag{3.47}$$

  All bodies: $$(J_1 + J_{sr} + J_{sl} + J_{sd} + J_5)\ \dot{\omega}_{sl} = T_{D3} \tag{3.48}$$

# 4 Computational Model

Matlab is used in order to simulate the synchronization process. As seen before in Chapter 3, each single phase has its own system of equations since the movements are different. For this reason, each one has been implemented in different functions, that is to say different m-files in Matlab.

The main program, that represents the process, calls every function separately. They are executed one after the other, thus a function is not active until the previous one has finished. Consequently, the end conditions can be used as initial conditions of the following phases.

In order to solve the systems of differential equations, the Matlab built-in ODE Solve *ode45* was used.

Upon introducing auxiliary equations for the second derivatives, the first-order system of ODEs has the following list of variables:

$$u = [\theta_g, \omega_g, x_{sr}, \theta_{sr}, \dot{x}_{sr}, \omega_{sr}, x_{sl}, \theta_{sl}, \dot{x}_{sl}, \omega_{sl}, x_{sd}, y_{sd}, \dot{x}_{sd}, \dot{y}_{sd}]^T$$

Where $\theta_g$, $\theta_{sr}$ and $\theta_{sl}$ are the angular displacements in rad of the clutch gear, synchro ring and sleeve, respectively.

One of the unknown parameters is the time needed for every phase. Therefore, every solver has the '*Event*' option activated so that *ode45* stops when a certain event occurs:

```
options=odeset('Events',@events,'Stats','on'); %Create an options variable
[t,u1]=ode45(@phase1,[t10 t1f],u10,options);
```

The stop conditions for the first three phases are:

- Phase 1: The strut detent has travelled the distance required to start pushing the synchro ring towards the clutch cone. An example of the code of this event can be seen below:

```
function [value,isterminal,direction]=events(t,u1)
    value=u1(11)-1e-3; %Stops when u1(11)=1e-3
    isterminal=1; %Stop after the first event (=0 to get all the events)
    direction=0; % No matter which direction (+ -> -  or - -> +)
end
```

- Phase 2: The synchro ring displacement has reached the maximum value and the conical surfaces are in contact.
- Phase 3: The angular velocities of the gear and the sleeve are equal.

For more information about de code in Matlab see Appendix 7.1.

## 4.1 Simulation results and discussion

### 4.1.1 Permissible values

Before starting with the simulation results, one should have in mind permissible values for the manual effort and the synchronization time (Lechner and Neunheimer, 1999), since these limits could be useful in or-

der to determine whether the design parameters and initial conditions are correct for the synchronization process.

On the one hand, the maximum effort that the driver is supposed to be able to apply has the following standard values: $F_{effort} = 180 - 250$ N

This value is not transmitted directly to the sleeve, but to the shifting mechanism that connects the shift lever and the synchronizer. This linkage has a transmission ratio ($TR$) that multiplies the magnitude of the effort and normally varies between 7:1 and 12:1. The other factor that affects this value is the efficiency of this linkage ($\eta_{link} < 70\%$). Consequently, the load applied to the sleeve can be expressed as:

$$F_{fork} = F_{effort} \cdot TR \cdot \eta_{link} \tag{4.1}$$

On the other hand, the slipping time permissible for commercial vehicles is between 0,25 and 0,4 seconds. This value refers only to the synchronization phase. However, since this project simulates this period, the resulting time can be compared directly with this magnitude.

### 4.1.2 Simulation results and discussion

As said in Section 1.2, one of the purposes of this model is to study the response by varying the values of some design parameters. In this Section these input variables that are going to be changed are: the cone angle ($\alpha_c$), the mean cone radius ($R_c$), the number of internal grooves in synchro ring ($n$), the axial load applied to the sleeve ($F_{fork}$) and the spring stiffness ($k_{spring}$). It is going to be analyzed the duration of the phases, the relative angular speed between the clutch body gear and the synchro ring and the axial and radial displacements as output variables. In this way, one can test whether the model responds in accordance with the claims in Section 2.2.4.

The input variables are going to be changed one by one maintaining the other values. Therefore, the magnitudes of these parameters when are not changed are:

| **Description** | **Unit** | **Value** |
|---|---|---|
| Spring stiffness | N/m | $8 \cdot 10^3$ |
| Cone angle | ° | 6 |
| Mean cone radius | mm | 75 |
| Number of internal grooves in synchro ring | - | 28 |

Table 4.1: *Initial simulation conditions.*

The axial force applied to the sleeve is considered to vary with time following the equation:

$$F_{fork} = 147 + 1155 \cdot t$$

In order to obtain this relation it has been considered a linkage efficiency of $\mu_{link} = 0,6\%$ and a transmission ratio of 7:1. In addition, it is supposed a starting effort of 35N and a maximum value of 90N reached in 0,2 seconds. The general statement of the equation would be:

$$F_{fork}(t) = F_{fork,0} + \frac{F_{fork,max} - F_{fork,0}}{t_{total}} t \tag{4.2}$$

It can be found in reference (Lovas et al., 2004).

The values of the other input variables of the model are included in the matlab code in the Appendix 7.1.

For this first sort of magnitudes the duration obtained for each phase is:

| | **Phase 1** | **Phase 2** | **Phase 3** | **Total** |
|---|---|---|---|---|
| **Time** [s] | 0,0013 | 0,0068 | 0,2301 | 0,2382 |

Table 4.2: *Duration of each phase for the initial simulation conditions.*

In the next Figure 4.1 it can be seen the axial displacements of the synchro ring, sleeve and strut detent and the radial displacement of the strut. Note that the x-axis has been shortening since the position of the three bodies during the third phase is constant.

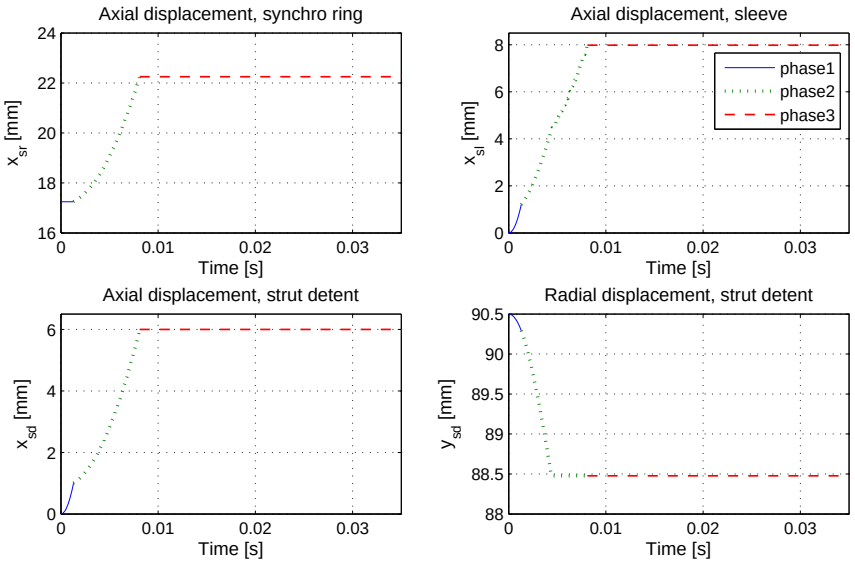


Figure 4.1: *Axial displacements of the different bodies and radial displacement of strut detent.*

It is observed that the spring is compressed and thus there is a relative displacement between the sleeve and the strut. Moreover, the synchro ring starts to move at the second phase and all the bodies remain in the same position during the synchronization phase.

On the following Figure 4.2 is represented the relative rotating speed between the clutch gear and the synchro ring and can be seen that the value is decreasing until the difference is zero, that is the end of the phase 3.

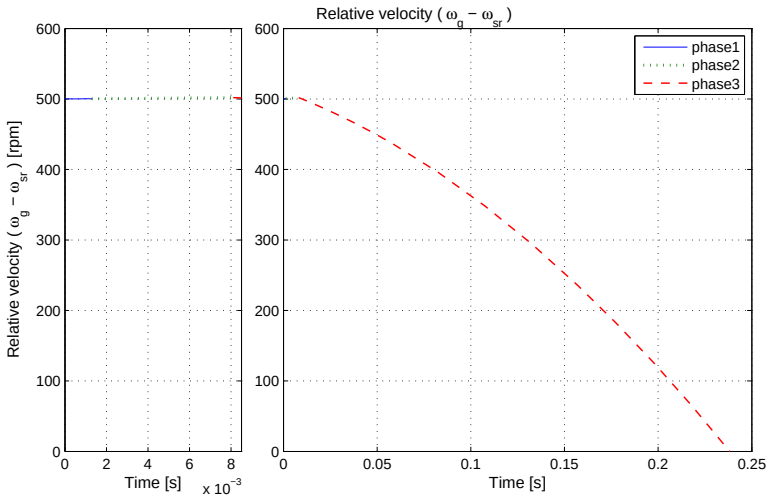


Figure 4.2: *Relative rotational speed for the initial simulation conditions.*

**Variation of the cone angle:**

| Cone angle | Phase 1 | Phase 2 | Phase 3 | Total |
|---|---|---|---|---|
| 6 ° | 0,0013 s | 0,0068 s | 0,2301 s | 0,2382 s |
| 6,5 ° | 0,0013 s | 0,0068 s | 0,2443 s | 0,2524 s |
| 7 ° | 0,0013 s | 0,0068 s | 0,2580 s | 0,2661 s |
| 7,5 ° | 0,0013 s | 0,0068 s | 0,2714 s | 0,2795 s |

Table 4.3: *Synchronization time for different values of the cone angle.*

The effect of the cone angle can be seen in the phase 3 and as stated in the literature review, the shifting time increases with this parameter. A lower value of this angle will lead to a higher frictional torque between the cone surfaces and thus the sycnhronizer will need less time to make equal the angular velocities. Nevertheless, one cannot forget the limit related to the coefficient of friction in order to avoid the locking of the system (see equation (2.7)).

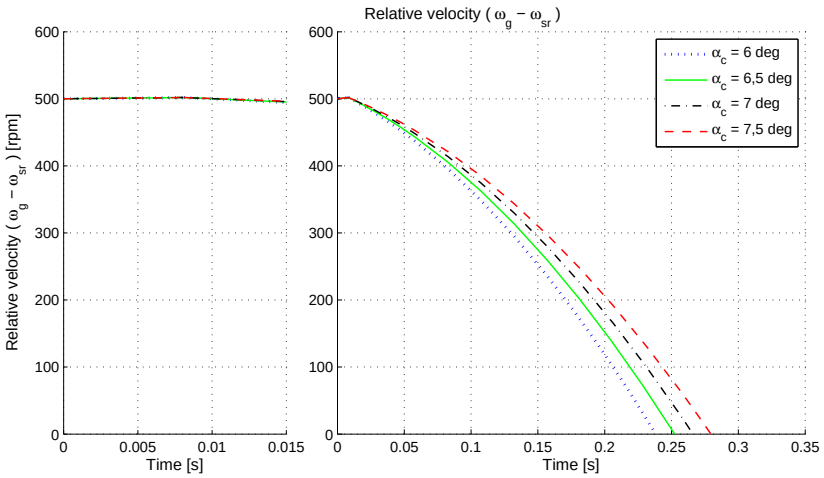


Figure 4.3: *Relative rotational speed for different values of the cone angle.*

Figure 4.3 shows the variation of the relative rotational velocity for different values of the cone angle.

**Variation of the mean cone radius:**

| Mean cone radius | Phase 1 | Phase 2 | Phase 3 | Total |
|---|---|---|---|---|
| 70 mm | 0,0013 s | 0,0068 s | 0,2423 s | 0,2504 s |
| 72 mm | 0,0013 s | 0,0068 s | 0,2373 s | 0,2454 s |
| 75 mm | 0,0013 s | 0,0068 s | 0,2301 s | 0,2382 s |
| 77 mm | 0,0013 s | 0,0068 s | 0,2256 s | 0,2337 s |

Table 4.4: *Synchronization time for different values of the mean cone radius.*

According to the results in Table 4.4, with a higher value of the mean cone radius it is obtained a lower synchronization time. This is due to the direct relation of this parameter and the friction torque, as seen in equation (2.4).

Figure 4.4 shows the variation of the relative rotational velocity for different values of the mean cone radius.

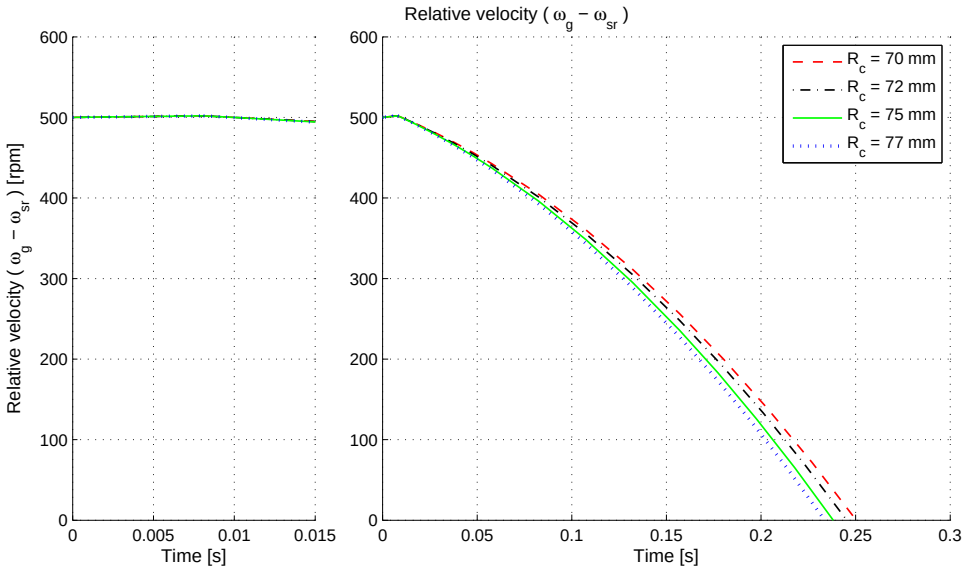


Figure 4.4: *Relative rotational speed for different values of the mean cone radius.*

**Variation of the number of grooves:**

| Num. grooves | Phase 1 | Phase 2 | Phase 3 | Total |
|---|---|---|---|---|
| 8 | 0,0013 s | - | - | - |
| 18 | 0,0013 s | - | - | - |
| 28 | 0,0013 s | 0,0068 s | 0,2301 s | 0,2382 s |
| 38 | 0,0013 s | 0,0068 s | 0,2302 s | 0,2383 s |

Table 4.5: *Synchronization time for different values of the number of grooves.*

In the case of 8 and 18 grooves the simulation is not able to finish the phase 2 with the initial simulation conditions. According to reference (Paffoni et al., 1997), the difficulty to break the oil film increases with the

decrease of the number of grooves. As a consequence, the required axial force applied to the sleeve has to increase since is not enought with the magnitude used.

Figure 4.5 corresponds to the variation of the relative rotational velocity for different values of the inner grooves of the synchro ring with the initial simulation conditions for the shift effort.

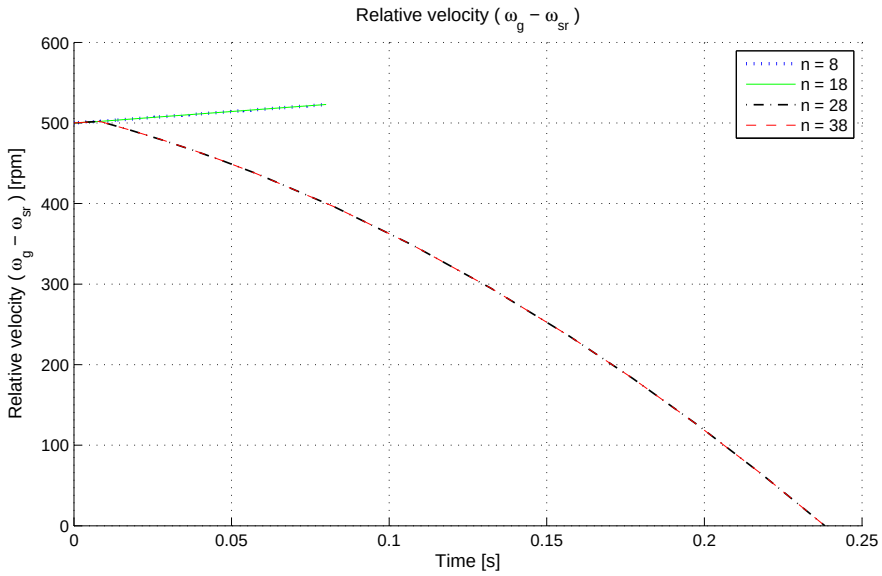


Figure 4.5: *Relative rotational speed for different values of the number of internal grooves (initial simulation conditions of axial effort applied).*

Now, trying to simulate the case $n = 18$ with a higher slope in the equation (4.2), a higher transmission ratio ($F_{effort,0} = 35$ N, $F_{effort,max} = 90$ N, $t_{total} = 0,01$ s and $TR = 12 : 1$) and maintaining the force constant during the third phase, the simulation is successful and the duration of the phases are shown in Table 4.6.

| **Num. grooves** | **Phase 1** | **Phase 2** | **Phase 3** | **Total** |
|---|---|---|---|---|
| 18 | 0,0010 s | 0,0383 s | 0,0335 s | 0,0728 s |

Table 4.6: *Synchronization time for n=18 and a higher shift effort.*

In this simulation, the shift effort has reached a maximum value of about 250 N that the driver has to apply. Therefore, with a reduced number of grooves a higher effort is required and, as a consequence, the synchronization time should be shorter. However, one should try not to exceed the permissible value of the manual effort.

In Figure 4.6 it can be seen the evolution of the relative velocity for this particular case.

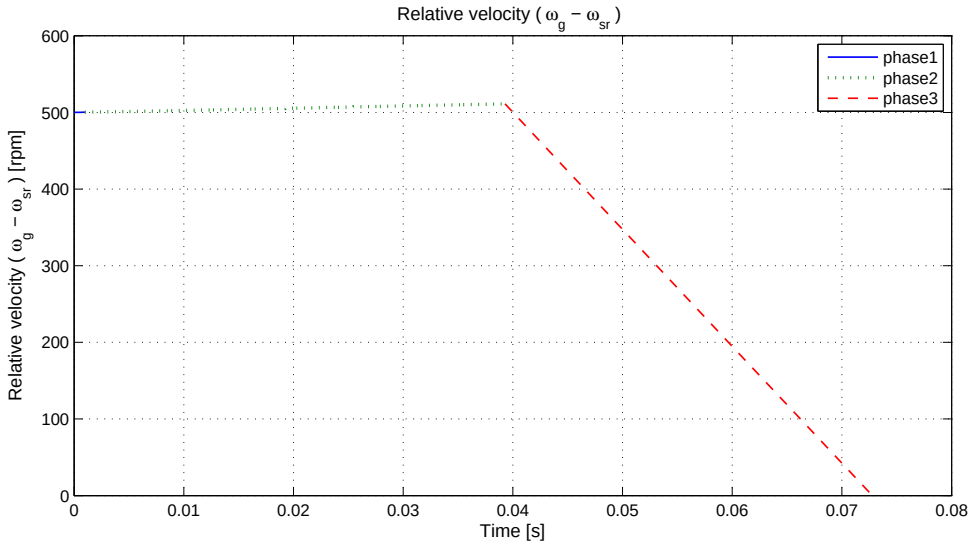


Figure 4.6: *Relative rotational speed for n=18.*

**Variation of the applied effort:**

The shift effort can be a constant value or have a linear increment as defined before. Consequently, in order to see the differences, both options were studied.

The first simulation takes the previous values as the maximum values for the equation (4.2). The minimum effort is maintained in 35 N.

| **Maximum manual effort** | **Phase 1** | **Phase 2** | **Phase 3** | **Total** |
|---|---|---|---|---|
| 50 N | 0,0013 s | 0,0067 s | 0,3474 s | 0,3554 s |
| 90 N | 0,0013 s | 0,0068 s | 0,2301 s | 0,2382 s |
| 140 N | 0,0013 s | 0,0067 s | 0,1787 s | 0,1867 s |
| 200 N | 0,0013 s | 0,0067 s | 0,1476 s | 0,1556 s |

Table 4.7: *Synchronization time for different values for maximum manual effort applied.*

Note that the simulated values for the load do not exceed the permissible values mentioned before.

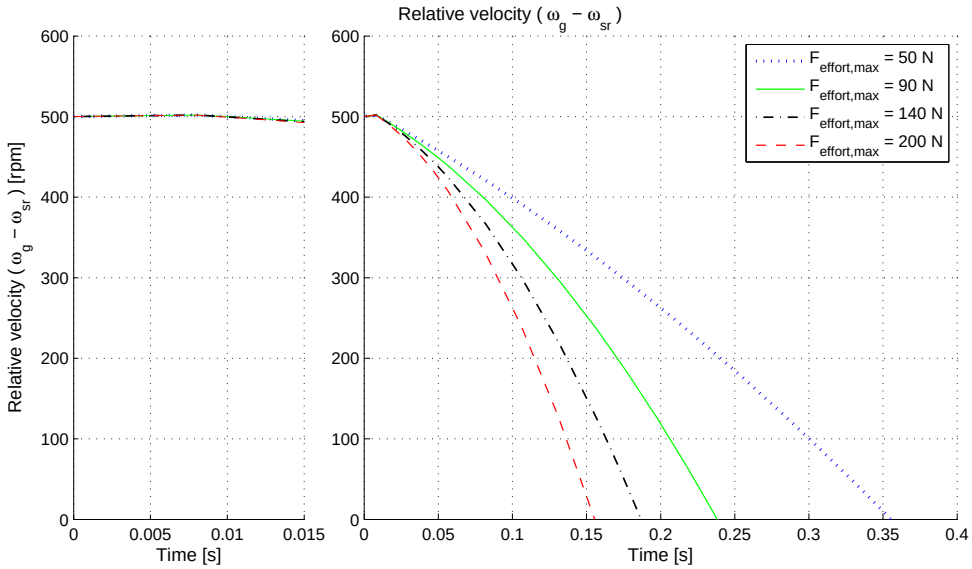


Figure 4.7: *Relative rotational speed for different values for the maximum effort applied.*

The second case is for a constant value of the load applied by the driver:

| **Manual effort** | **Phase 1** | **Phase 2** | **Phase 3** | **Total** |
|---|---|---|---|---|
| 50 N | 0,0011 s | 0,0058 s | 0,3367 s | 0,3454 s |
| 90 N | 0,0008 s | 0,0043 s | 0,1705 s | 0,1756 s |
| 140 N | 0,0006 s | 0,0035 s | 0,1053 s | 0,1094 s |
| 200 N | 0,0005 s | 0,0029 s | 0,0722 s | 0,0756 s |

Table 4.8: *Synchronization time for different values for a constant manual effort.*

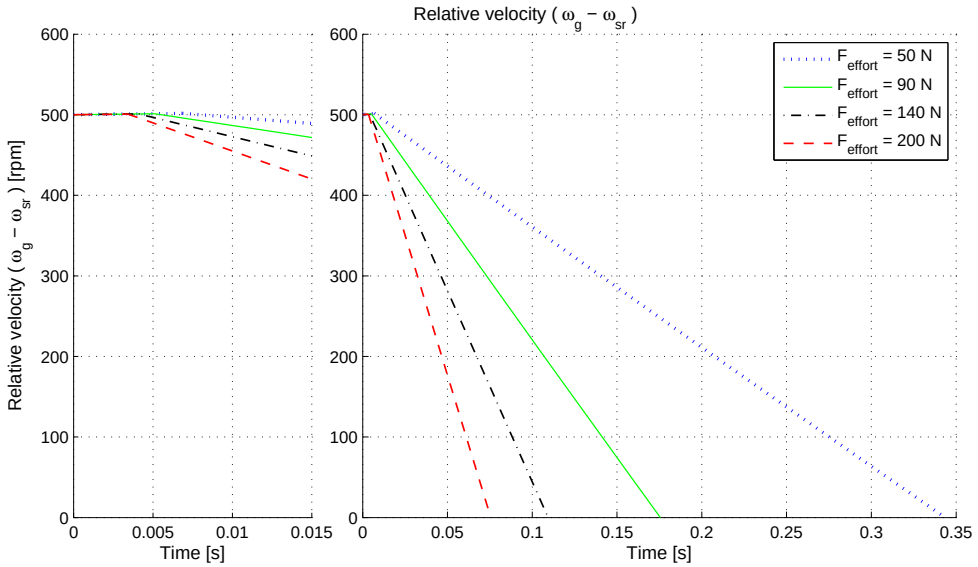


Figure 4.8: *Relative rotational speed for different values for a constant manual effort.*

In both conditions of the applied load it can be found out that with larger axial force a shorter time is obtained. Since the shift effort is related to the synchronizer torque, the higher the load will be the higher torque and consequently the shorter time.

**Variation of the spring stiffness:**

| Spring stiffness | Phase 1 | Phase 2 | Phase 3 | Total |
|---|---|---|---|---|
| $8 \cdot 10^3$ N/m | 0,0013 s | 0,0068 s | 0,2301 s | 0,2382 s |
| $15 \cdot 10^3$ N/m | 0,0063 s | 0,0150 s | 0,2222 s | 0,2435 s |
| $30 \cdot 10^3$ N/m | 0,0063 s | 0,0148 s | 0,2223 s | 0,2434 s |
| $45 \cdot 10^3$ N/m | 0,0053 s | 0,0148 s | 0,2223 s | 0,2434 s |

Table 4.9: *Synchronization time for different values of the spring stiffness.*

Table 4.9 shows that with the variation of this parameter there is not great difference in the duration of the phases simulated, but in the different displacements of the bodies (see Figure 4.9). Again the x-axis has been shortening.

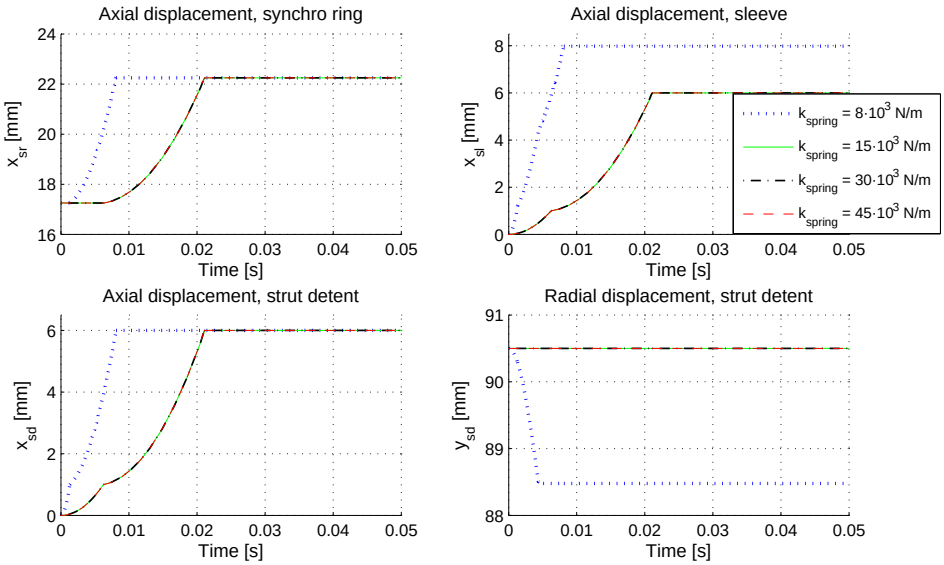


Figure 4.9: *Axial displacements of the different bodies and radial displacement of strut detent for different values of the spring stiffness.*

# 5 Conclusion and Outlook

This project was aimed to get a better knowledge of the synchronization processes and synchronizers. It has identified quality factors such as the shift comfort and shifting time, as well as the problems that could appear such as double bump and stick-slip phenomenon. It has also provided a list of significant parameters of the design that affect in different ways to the process.

In addition, the first three stages of the process have been simulated using Matlab, and the equations of motion have been established for the remaining five stages. The computational model seems to give reasonable responses to the variation of some significant parameters, such as the cone angle, the mean cone radius, the number of internal grooves in synchro ring, the shift force and the spring stiffness, and the effects of them are the expected ones according to the literature review. In fact, they agree with an increase of the friction torque and thus a shortening of the shifting time by reducing the cone angle or by increasing the mean cone radius and the axial force applied to the sleeve.

According to this model and the assumptions made for the values of the input parameters, the results show that an increase of the cone angle of less than 1° can increase the duration up to 12% taking as reference the initial simulation conditions. In the case of the mean cone radius a difference of 2 mm bigger, that is about 3% more frictional torque, could improve the synchronization time by 2%. The modification of both parameters does not affect the trend of the curve of the Relative velocity vs. Time. However, the behavior of these curves when changing the applied load is different. While increasing the maximum effort applied (case of variable force) the relative velocity tends to zero more abruptly. The same for a constant manual effort, but on this occasion the relative velocity decreases linearly in all the variations. In the case of the number of inner grooves it has been seen that with a lower value the axial shift effort has to increase rapidly and reaches a higher magnitude. As a result, the synchronization is done in less time. On the contrary, with more grooves there is a point where there is almost no difference in the resistance force of the oil film and thus in the synchronization time.

However, the values of some output variables, for instance the axial velocities of the sleeve, synchro ring and strut detent, are higher than the used in literature. Although this difference could be explained by the use of non-real design values, it cannot yet be concluded that the model is valid and could be used to simulate shifting processes for manual transmissions in commercial vehicles.

Consequently, further work is needed in order to finish and validate the model in Matlab with real data of both design parameters and input variables. This would allow to simulate the whole process and to study the second bump and stick-slip phenomenon to minimize their negative effect in the performance of the synchronizer.

Nevertheless, if one wants to go further with the model, the estimation of the drag torque could be changed by more detailed models that may provide better and more accurate results. Moreover, it could be studied whether the temperature and viscosity can be considered as constant during the process. The model of the synchronizer could also include the effect of boost surfaces and even offer the option to add more conical surfaces in order to increase the frictional torque. Besides, one could introduce the influence of the conicity angle error and thus the possible deformation of the synchro ring due to dissipated friction energy.

Finally, it could be adopted a "constraint" formulation of the system, i.e. to consider all the bodies at all stages, and then impose constraints depending on the phase. This would simplify the derivations of the equations but would require more careful numerical procedure (*ode45* would probably not suffice).

# 6 References


1. Abdel-Halim, N. A., Barton, D. C., Crolla, D. A. and Selim, A. M. (2000): *Performance of multicone synchronizers for manual transmissions.* Proceedings of the Institution of Mechanical Engineering. Part D: J. Automotive Engineering, Vol. 214, pp. 55-65, 2000.

2. Abel, A., Schreiber, U. and Schindler, J. (2006): *Engine and Gearbox Modeling and Simulation for Improving the Shifting Behaviour of Powertrains with Manual or Automated Transmissions.* Technical Report 2006-01-1641. SAE Technical Paper Series. 2006.

3. Back, O.: *Potentials for Efficiency Improvement out of the Synchronizer.* HOERBIGER Antriebstechnik GmbH Schongau, Germany.

4. Berglund, J. (2012): *Design of a power loss model for vehicle drivetrains.* Master's Thesis. Luleå University of Technology, Department of Engineering Sciences and Mathematics. Luleå, Sweden, 2012.

5. Gong, Z., Zhang, W., Chen, G. and Wang, W. (2008): *Analyses and Evaluation on Synchronizer of Manual Transmission.* Pacific-Asia Workshop on Computational Intelligence and Industrial Application. Vol. 1, December 2008, pp. 842-845.

6. Gustavsson, A. (2009): D*evelopment and Analysis of Synchronization Process Control Algorithms in a Dual Clutch Transmission.* Master's Thesis. Linköping University of Technology, LITH-ISY-EX—09/4191—SE. Linköping, Sweden, 2009.

7. Häggström, D. and Nordlander, M. (2011): *Development of a Program for Calculating Gearbox Synchronization.* Master's Thesis, Luleå University of Technology. Luleå, Sweden, 2011.

8. Hedman, A. (2011): Powertrain mechanics, course 2011-2012. Chalmers University of Technology, Applied Mechanics department. Göteborg, Sweden.

9. Hoshino, H. (Nissan Diesel Motor Co., Ltd.)(1999): *Analysis on Synchronization Mechanism of Transmission.* Technical Report 1999-01-0734. SAE Technical Paper Series. Detroit, MI, USA, 1999.

10. Kelly, D. and Kent, C. (2000): *Gear Shift Quality Improvement in Manual Transmissions Using Dynamic Modelling.* Paper presented at FISITA World Automotive Congress, Seoul, Korea. June 2000.

11. Kim, J., Sung, D., Seok, C., Kim, H., Song, H., Lim, C. and Kim, J. (2002): *Development of Shift Feeling Simulator for a Manual Transmission.* Technical Report 2001-01-2202. SAE Technical Paper Series. Paris, France, 2002.

12. Lechner, G. And Neunheimer, H. (1999): *Automotive Transmissions: Fundamentals, Selection, Design and Application.* Springer, Germany. 448 pp.

13. Liu, Y-C. and Tseng, C-H. (2007): *Simulation and Analysis of synchronisation and engagement on manual transmission gearbox.* Int. J. Vehicle Design, Vol. 43, No. 1-4, pp. 200-220, 2007.

14. Lovas, L. (2004): *Etude des relations entre le comportment et la fabrication des synchronisateurs des boîtes de vitesses manuelles.* PhD Thesis. L'Institut National des Sciences Appliquées de Lyon, 2004.

15. Lovas, L., Play, D., Mariligeti, J. and Rigal, J.-F. (2006): *Mechanical Behaviour Simulation for Synchromesh Mechanism Improvements.* Proc. IMechE, Part D: J. Automobile Engineering, 2006, Vol. 220, pp. 919-945.

16. Lovas, L., Play, D., Mariligeti, J. and Rigal, J.-F. (2005): *Modelling of Gear Changing Behaviour.* Periodica Polytechnica Ser. Transp. Eng. Vol. 34, No. 1-2, July 2005, pp. 35-58.

17. Paffoni, B., Progri, R., Gras, R. (2000): *The mixed phase of gearbox synchromesh operation.* Proc. IMechE, Part J: J. Engineering Tribology, Vol. 214, pp. 157-165, 2000.

18. Paffoni, B., Progri, R., Gras, R. and Blouët, J. (1995): *The hydrodynamic phase of gearbox synchromesh operation: The influence of radial and circumferential grooves.* Proceedings of the Institution of Mechanical Engineering. Part J: Journal of Engineering Tribology, Vol. 211, pp. 107-116, 1997.

19. Razzacki, S. T. (DaimlerChrysler Inc.) and Hottenstein, J. E. (FEV Corpation) (2007): *Synchronizer Design and Development for Dual Clutch Transmission (DCT).* Technical Report 2007-01-0114, SAE Technical Paper Series, 2007.

20. Razzacki, S. T. (DaimlerChrysler Inc.) (2004): *Synchronizer Design: A Mathematical and Dimensional Treatise.* Technical Report 2001-01-1230. SAE Technical Paper Series, 2004. Reprinted from: Transmission & Driveline Symposium 2004 (SP-1817).

21. Rosen, I., Kruk, S., Eker, P. O. and Mellgren, H. (AB Volvo, 1969-70): *Synchromesh Mechanisms: Experience of Heavy Truck Gearboxes.* Proceedings of the Institution of Mechanical Engineering. Vol. 184, Pt 31, pp. 438-476, 1969-70.

22. Sandooja, A. (2012): *Double Indexing Synchronizer – To Amplify the Synchronizer Capacity.* Technical Report 2012-01-2003, SAE International. 2012.

23. Schaeffler KG, INA (2007): *Intermediate Rings for Multi-Cone Synchronizer Systems.* Automotive Product Information API 06. Germany. August, 2007.

24. Sharma, M. K. and Salva, J. (2012): *Shift System Inertia Mass Optimization Techniques to Minimize Double Bump for Manual Transmission.* Technical Report 2012-01-1999. SAE International. 2012.

25. Spreckels Marcus (Sulzer Friction Systems) (2012): *Improved synchronization in vehicle transmissions.* Sulzer Technical Review. Bremen, Germany, 2012.

26. Spreckels, M. (2001): *Einfluss der Temperaturverteilung auf das tribologische Verhalten von Synchronisierungen.* PhD Thesis, University of Hannover, 2001.

27. Vettorazzo, D., Gama, D., Fernandez, J. and Rodrigues, P. (2006): *Manual Transmission: Synchronization Main Aspects.* Technical Report 2006-01-2519, SAE Technical Papers Series, 2006.

28. Yuming, G. (2011): *Discuss Designing-Method of Transmission Synchronizer.* Datong Gear Co. Ltd, China National Heavy Duty Truck Group. Datong, China. 2011.

## 6.1 Patents

29. Bader, J. (2008): *Synchronizer for a manual transmission especially for a motor vehicle.* U.S. Patent No. 7,431,137 B2

30. Braun, E. R. (1996): *Synchronizer with self-energizing.* U.S. Patent No. 5,544,727

31. Christoffer, U. and Spreckels, M. (2013): *Synchronizing ring.* U.S. Patent No. 8,342,307 B2

32. Coxon, D. J. and Jackson, G. A. (2006): *Synchronizer.* U.S. Patent No. 7,131,521 B2

33. Daizuke Saito, O., Yukio Ueda, T. and Yuji Gatade, Y. (2011): *Synchronizer device.* U.S. Patent No. 8,020,682 B2

34. Hughes, D. A. (1998): *Synchronizer.* U.S. Patent No. 5,738,194

35. Loeffler, J. M. (1996): *Multiple cone synchronizer for vehicle transmission.* U.S. Patent No. 5,560,461

36. Nilsson, D. (SCANIA CV AB)(2001): *Synchronizing device for a planet gear.* Swedish Patent No. WO 01/55620

37. Olsson, R. (AB VOLVO)(1997): *Synchronizing device in a vehicle gearbox.* Swedish Patent No. WO 97/49934

# 7 Appendix

## 7.1 Matlab code

**Phase 1:**

```
function P1=phase1(t,u)
%Motion equations phase 1: First free fly
%Input variables:
u=[1)phitag,2)wg,3)xsr,4)phitasr,5)dxsr,6)wsr,7)xsl,8)phitasl,9)dxsl,1
0)wsl,11)xsd,12)ysd,13)dxsd,14)dysd]'

%Rotating inertias [kg·m^2] and mass [kg]
J1=0.17;
Jsr=4.0258e-3;
Jsl=1.4413e-2;
Jsd=5.4717e-4;
J5=6.1429e-2*2;
msl=2.754;
np=3; %Number of strut detents
msd=0.166/np;

l5=17.2e-3;
l6=93.25e-3;
l7=106.3e-3;

phi=45*pi/180; %Ramp angle [rad]
def_spring0=5e-3; %Initial deformation of detent spring (neutral
position) [m]
ysd0=95.5e-3; %Position of the detent ball if the spring was not
compressed [m]

cdrag1=0.02; %Oil viscous damping [kg m^2)/s]
cdrag3=0.03; %Oil viscous damping [kg m^2)/s]

Feff=35; %Load applied by the driver at the shift lever [N], Maximum
value allowed: 180-250 N
Feff_max=90; %Max effort applied by the driver [N]
eff=0.6; %Efficiency of the shift mechanism (normally <70%)
TR=7; %Transmission ratios of the shift mechanism (Normally varies
between 7:1 and 12:1)
Ffork0=Feff*eff*TR; %Load on the sleeve [N]
Ffork_max=Feff_max*eff*TR; %Max load on the sleeve [N]
Inc_Ffork=(Ffork_max-Ffork0)/0.2;

Ffork=Ffork0+Inc_Ffork*t;

musl=0.1; %Friction coef. between ball and sleeve
kspring=8000;
%kspring=Ffork0*(cos(phi)-
musl*sin(phi))/(np*def_spring0*(musl*cos(phi)+sin(phi))); %Spring rate
[N/m], (~13911 N/m with Feff=30 N)

%----------------------------Motion equations-------------------------
----
    %Change of variable:
```

```
%P1=zeros(14,1);
%P1=[1)wg,2)dwg,3)dxsr,4)wsr,5)ddxsr,6)dwsr,7)dxsl,8)wsl,9)ddxsl,10)dw
sl,11)dxsd,12)dysd,13)ddxsd,14)ddysd]'

wg=u(2); %wg
dwg=-1/J1*(cdrag1*wg); %dwg
dxsr=u(5); %dxsr
wsr=u(6); %wsr
ddxsr=0; %ddsxr
dxsl=u(9); %dxsl
wsl=u(10); %wsl

dwsl=-(cdrag3*wsl)/(Jsr+Jsl+Jsd+J5); %dwsl
dwsr=dwsl; %dwsr=dwsl


Fspring=kspring*((ysd0-65e-3)-sqrt((u(11)^2+(u(12)-65e-3)^2)));
%Spring load considering the bending of the spring [N]
                                                              %The
magnitude of the Fspring will vary if the spring is compressed or
relaxed


Nsl=(Ffork*l7)/(musl*l5*sin(phi)+l6*sin(phi)+musl*l6*cos(phi)-
l5*cos(phi));

%The strut detent cannot move upwards, it has no space
if (Fspring+(Nsl/np)*(musl*sin(phi)-cos(phi)))>=0
    ddysd=0; %ddysd=0
    dysd=0; %dysd=0
    ddxsl=Ffork/(msl+np*msd); %ddxsl
    ddxsd=ddxsl; %ddxsd=ddxsl
    u(13)=u(9);
    dxsd=u(13); %dxsd
else
    dysd=u(14); %dysd
    ddysd=1/msd*(Fspring+(Nsl/np)*(musl*sin(phi)-cos(phi))); %ddysd
    ddxsd=(1/(np*msd))*Nsl*(sin(phi)+musl*cos(phi)); %ddxsd
    ddxsl=ddxsd+abs(ddysd/tan(phi)); %ddxsl
    dxsd=u(13); %dxsd
end
P1=[wg;dwg;dxsr;wsr;ddxsr;dwsr;dxsl;wsl;ddxsl;dwsl;dxsd;dysd;ddxsd;ddy
sd];
end
```

**Phase 2:**

```
%Assumption: xsd moves with xsr but separately from xsl

function P2=phase2(t,u)
%Motion equations phase 2: Start of angular velocity synchronization
%Input variables:
u=[1)phitag,2)wg,3)xsr,4)phitasr,5)dxsr,6)wsr,7)xsl,8)phitasl,9)dxsl,1
0)wsl,11)xsd,12)ysd,13)dxsd,14)dysd]'

%Rotating inertias [kg·m^2] and mass (kg)
J1=0.17;
Jsr=4.0258e-3;
Jsl=1.4413e-2;
Jsd=5.4717e-4;
J5=6.1429e-2*2;
msr=1.127;
msl=2.754;
np=3; %Number of strut detents
msd=0.166/np;

Rc=75e-3; %Mean cone radius [m]
Rh=89.95e-3; %Radius of contact between synchro hub and synchro ring
[m]
Rsd=90.4e-3; %Radius of contact between synchro ring and strut detent
[m]
b=6.95e-3; %Half length of cone generatrix [m]
n=28; %Number of circumferential grooves
a=0.15e-3; %Half width of a groove on the cone surface [m]
alphac=6*pi/180; %Cone angle [rad]
phi=45*pi/180; %Ramp angle [rad]
def_spring0=5e-3; %Initial deformation of detent spring (neutral
position) [m]
ysd0=95.5e-3; %Position of the detent ball if the spring was not
compressed [m]

l1=1e-3;
l2=15.75e-3;
l3=3.95e-3;
%l4=17.25e-3;
l5=17.2e-3;
l6=93.25e-3;
l7=106.3e-3;

cdrag1=0.02; %Oil viscous damping [kg·m^2/s]
cdrag2=0.03; %Oil viscous damping [kg·m^2/s]
cdrag3=0.03; %Oil viscous damping [kg·m^2/s]

h0=5e-3*sin(alphac); %Oil thickness (Normal distance between cone
surfaces), initial distance [m]
h1=1e-3*sin(alphac); %Oil thickness (Normal distance between cone
surfaces), start viscosity stage [m]
hmin=1e-6*sin(alphac); %Oil thickness (Normal distance between cone
surfaces), final distance [m]
dynvis=1.8e-5*839.4; %Dynamic viscosity [Pa·s] ATF at 60°C
musd=0.1; %Friction coef. between strut and synchro ring
musl=0.1; %Friction coef. between strut and sleeve
muc=0.02; %Friction coef. between cone surfaces
```

```
Feff=35; %Load applied by the driver at the shift lever [N], Maximum
value allowed: 180-250 N
Feff_max=90; %Max effort applied by the driver [N]
eff=0.6; %Efficiency of the shift mechanism (normally <70%)
TR=7; %Transmission ratios of the shift mechanism (Normally varies
between 7:1 and 12:1)
Ffork0=Feff*eff*TR; %Load on the sleeve [N]
Ffork_max=Feff_max*eff*TR; %Max load on the sleeve [N]
Inc_Ffork=(Ffork_max-Ffork0)/0.2;

kspring=8000;
%kspring=Ffork0*(cos(phi)-
musl*sin(phi))/(np*def_spring0*(musl*cos(phi)+sin(phi))); %Spring rate
[N/m], (~13911 N/m with Feff=30 N)

%-----------------------------Equations-------------------------------
----

%Influence of circumferential grooves and oil thickness
bi=b-(n/2)*a;
Kcc=1+(1-n)*(a/bi);
if Kcc<0
    Kcc=0;
else
    Kcc=1+(1-n)*(a/bi);
end

Knc=(1/n^2)*(1+(1-n)*(a/bi))^3;
if Knc<0
    Knc=0;
else
    Knc=(1/n^2)*(1+(1-n)*(a/bi))^3;
end

%-------------------------Motion equations-----------------------------
-----
    %Change of variable:
%P2=zeros(14,1);
%P2=[1)wg,2)dwg,3)dxsr,4)wsr,5)ddxsr,6)dwsr,7)dxsl,8)wsl,9)ddxsl,10)dw
sl,11)dxsd,12)dysd,13)ddxsd,14)ddysd]'

h=h0-((u(3)-17.25e-3)*sin(alphac));
Fspring=kspring*((ysd0-65e-3)-sqrt((u(11)^2+(u(12)-65e-3)^2)));
%Spring load considering the bending of the spring [N]
                                                              %The
magnitude of the Fspring will vary if the spring is compressed or
relaxed

Ffork=Ffork0+Inc_Ffork*t;

if h>h1 && h<=h0
    %Ffork=Ffork0+Inc_Ffork*t;
    wg=u(2); %wg
    dwg=-1/J1*cdrag1*wg; %dwg

    wsr=u(6); %wsr
    dwsl=-(1/(Jsr+Jsl+Jsl+J5))*cdrag2*wsr; %dwsl
    dwsr=dwsl; %dwsr=dwsl
    wsl=u(10); %wsl
```

```
    Nsl=(Ffork*l7)/(musl*l5*sin(phi)+l6*sin(phi)+musl*l6*cos(phi)-
l5*cos(phi));
    %Nsd=(Nsl/l3)*(l2*cos(phi)-l1*sin(phi)-musl*l1*cos(phi)-
musl*l2*sin(phi));

    if (Fspring+(Nsl/np)*(musl*sin(phi)-cos(phi)))>=0 %The strut
detent cannot move upwards (design constraint)
        dysd=0; %dysd=0
        ddysd=0; %ddysd=0
        dxsl=u(9); %dxsl
        dxsr=dxsl; %dxsr=dxsl
        dxsd=dxsl; %dxsd=dxsl
        ddxsl=(1/(msr+msl+np*msd))*Ffork; %ddxsl
        ddxsr=ddxsl; %ddxsr=ddxsl
        ddxsd=ddxsl; %ddxsd=ddxsl
    else
        dysd=u(14); %dysd
        ddysd=1/msd*(Fspring+(Nsl/np)*(musl*sin(phi)-cos(phi)));
%ddysd
        dxsl=u(9); %dxsl
        dxsd=u(13); %dxsd
        dxsr=dxsd; %dxsr=dxsd
        ddxsr=1/(msr+np*msd)*(Nsl*(sin(phi)+musl*cos(phi))); %ddxsr
        ddxsd=ddxsr; %ddxsd=ddxsr
        ddxsl=ddxsd+(abs(ddysd)/tan(phi)); %ddxsl
        if u(7)-u(11)>=2e-3
            ddysd=0; %ddysd=0
            dysd=0; %dysd=0
            ddxsl=0; %ddxsl=0
            dxsl=0; %dxsl=0
        end
        if u(12)<=90.5e-3-(2e-3*tan(phi))
            u(12)=90.5e-3-(2e-3*tan(phi));
            ddysd=0;
            dysd=0;
        end
    end

elseif h==h1
    %Ffork=Ffork0+Inc_Ffork*t;

    wg=u(2); %wg
    wsr=u(6); %wsr
    wsl=u(10); %wsl

    Nsl=(Ffork*l7)/(musl*l5*sin(phi)+l6*sin(phi)+musl*l6*cos(phi)-
l5*cos(phi));
    Nsd=(Nsl/l3)*(l2*cos(phi)+musl*l1*cos(phi)+l1*sin(phi)-
musl*l2*sin(phi));

    if (Fspring+(Nsl/np)*(musl*sin(phi)-cos(phi)))>=0 %The strut
detent cannot move upwards (design constraint)
        dysd=0; %dysd=0
        ddysd=0; %ddysd=0
        dxsl=u(9); %dxsl
        dxsr=dxsl; %dxsr=dxsl
        dxsd=dxsl; %dxsd=dxsl
```

```
        Ncax=Knc*16*pi*dynvis*dxsr*(sin(alphac))^2*Rc*(b/h)^3; %Axial
force applying hydrodynamics laws
        Nh=Nsd*musd-(Ncax/sin(alphac))*muc;

        Tc=Kcc*4*pi*dynvis*dxsr*Rc^3*wsr*(b/h)*(1-(wg/wsr)); %Friction
torque applying hydrodynamics laws
        dwg=-1/J1*(abs(Tc)+cdrag1*wg); %dwg
        dwsr=1/Jsr*(abs(Tc)+Nh*Rh-Nsd*musd*Rsd-cdrag2*wsr); %dwsr
        dwsl=(1/(Jsl+Jsd+J5))*(Nsd*musd*Rsd-Nh*Rh-cdrag3*wsl); %dwsl

        ddxsl=(1/(msr+msl+np*msd))*(Ffork-
Ncax*(1+muc*(cos(alphac)/sin(alphac)))); %ddxsl
        ddxsr=ddxsl; %ddxsr=ddxsl
        ddxsd=ddxsl; %ddxsd=ddxsl
    else
        dysd=u(14); %dysd
        ddysd=1/msd*(Fspring+(Nsl/np)*(musl*sin(phi)-cos(phi)));
%ddysd
        dxsl=u(9); %dxsl
        dxsd=u(13); %dxsd
        dxsr=dxsd; %dxsr=dxsd

        Ncax=Knc*16*pi*dynvis*dxsr*(sin(alphac))^2*Rc*(b/h)^3; %Axial
force applying hydrodynamics laws
        Nh=Nsd*musd-(Ncax/sin(alphac))*muc;

        Tc=Kcc*4*pi*dynvis*dxsr*Rc^3*wsr*(b/h)*(1-(wg/wsr)); %Friction
torque applying hydrodynamics laws
        dwg=-1/J1*(abs(Tc)+cdrag1*wg); %dwg
        dwsr=1/Jsr*(abs(Tc)+Nh*Rh-Nsd*musd*Rsd-cdrag2*wsr); %dwsr
        dwsl=(1/(Jsl+Jsd+J5))*(Nsd*musd*Rsd-Nh*Rh-cdrag3*wsl); %dwsl

        ddxsr=1/(msr+np*msd)*(Nsl*(sin(phi)+musl*cos(phi))-
Ncax*(1+muc*(cos(alphac)/sin(alphac)))); %ddxsr
        ddxsd=ddxsr; %ddxsd=ddxsr
        ddxsl=ddxsd+(abs(ddysd)/tan(phi)); %ddxsl
        if u(7)-u(11)>=2e-3
            ddysd=0; %ddysd=0
            dysd=0; %dysd=0
            ddxsl=0; %ddxsl=0
            dxsl=0; %dxsl=0
        end
        if u(12)<=90.5e-3-(2e-3*tan(phi))
            u(12)=90.5e-3-(2e-3*tan(phi));
            ddysd=0;
            dysd=0;
        end
    end

elseif h<h1 && h>hmin
    %Ffork=Ffork0+Inc_Ffork*t;

    wg=u(2); %wg
    wsr=u(6); %wsr
    wsl=u(10); %wsl

    Nsl=(Ffork*l7)/(musl*l5*sin(phi)+l6*sin(phi)+musl*l6*cos(phi)-
l5*cos(phi));
    %Nsd=(Nsl/l3)*(l2*cos(phi)-l1*sin(phi)-musl*l1*cos(phi)-
musl*l2*sin(phi));
```

```
    if (Fspring+(Nsl/np)*(musl*sin(phi)-cos(phi)))>=0 %The strut
detent cannot move upwards (design constraint)
        dysd=0; %dysd=0
        ddysd=0; %ddysd=0
        dxsl=u(9); %dxsl
        dxsr=dxsl; %dxsr=dxsl
        dxsd=dxsl; %dxsd=dxsl

        Tc=Kcc*4*pi*dynvis*dxsr*Rc^3*wsl*(b/h)*(1-(wg/wsl)); %Friction
torque applying hydrodynamics laws
        dwg=-1/J1*(abs(Tc)+cdrag1*wg); %dwg
        dwsl=(1/(Jsr+Jsl+Jsd+J5))*(abs(Tc)-cdrag3*wsl); %dwsl
        dwsr=dwsl; %dwsr=dwsl

        Ncax=Knc*16*pi*dynvis*dxsr*(sin(alphac))^2*Rc*(b/h)^3;

        ddxsl=(1/(msr+msl+np*msd))*(Ffork-
Ncax*(1+muc*(cos(alphac)/sin(alphac)))); %ddxsl
        ddxsr=ddxsl; %ddxsr=ddxsl
        ddxsd=ddxsl; %ddxsd=ddxsl

    else
        dysd=u(14); %dysd
        ddysd=1/msd*(Fspring+(Nsl/np)*(musl*sin(phi)-cos(phi)));
%ddysd

        dxsl=u(9); %dxsl
        dxsd=u(13); %dxsd
        dxsr=dxsd; %dxsr=dxsd

        Tc=Kcc*4*pi*dynvis*dxsr*Rc^3*wsl*(b/h)*(1-(wg/wsl)); %Friction
torque applying hydrodynamics laws
        dwg=-1/J1*(abs(Tc)+cdrag1*wg); %dwg
        dwsl=(1/(Jsr+Jsl+Jsd+J5))*(abs(Tc)-cdrag3*wsl); %dwsl
        dwsr=dwsl; %dwsr=dwsl

        Ncax=Knc*16*pi*dynvis*dxsr*(sin(alphac))^2*Rc*(b/h)^3;

        dxsd=u(13); %dxsd
        ddxsr=1/(msr+np*msd)*(Nsl*(sin(phi)+musl*cos(phi))-
Ncax*(1+muc*(cos(alphac)/sin(alphac)))); %ddxsr
        ddxsd=ddxsr; %ddxsd=ddxsr
        ddxsl=ddxsd+(abs(ddysd)/tan(phi)); %ddxsl
        if u(7)-u(11)>=2e-3
            ddysd=0; %ddysd=0
            dysd=0; %dysd=0
            ddxsl=0; %ddxsl=0
            dxsl=0; %dxsl=0
        end
        if u(12)<90.5e-3-(2e-3*tan(phi))
            u(12)=90.5e-3-(2e-3*tan(phi));
            ddysd=0;
            dysd=0;
        end
    end

elseif h<=hmin
    %Ffork=Ffork0+Inc_Ffork*t;
```

```
    h=hmin;
    wg=u(2); %wg
    dxsr=0; %dxsr
    wsr=u(6); %wsr
    ddxsr=0; %ddxsr
    wsl=u(10); %wsl
    dxsd=0; %dxsd
    ddxsd=0; %ddxsd

    Tc=Kcc*4*pi*dynvis*dxsr*Rc^3*wsl*(b/h)*(1-(wg/wsl)); %Friction
torque applying hydrodynamics laws
    dwg=-1/J1*(abs(Tc)+cdrag1*wg); %dwg

    dwsl=(1/(Jsr+Jsl+Jsd+J5))*(abs(Tc)-cdrag3*wsl); %dwsl
    dwsr=dwsl; %dwsr=dwsl

    Nsl=(Ffork*l7)/(musl*l5*sin(phi)+l6*sin(phi)+musl*l6*cos(phi)-
l5*cos(phi));
    %Nsd=(Nsl/(musd*l4+l3))*(l2*cos(phi)-l1*sin(phi)-musl*l1*cos(phi)-
musl*l2*sin(phi));

    if (Fspring+(Nsl/np)*(musl*sin(phi)-cos(phi)))>=0 %The strut
detent cannot move upwards (design constraint)
        dysd=0; %dysd=0
        ddysd=0; %ddysd=0
        dxsl=0;
        ddxsl=0;
    else
        dysd=u(14); %dysd
        ddysd=1/msd*(Fspring+(Nsl/np)*(musl*sin(phi)-cos(phi)));
%ddysd
        dxsl=u(9);
        ddxsl=ddxsd+(abs(ddysd)/tan(phi)); %ddxsl
        if u(7)-u(11)>=2e-3
            ddysd=0; %ddysd=0
            dysd=0; %dysd=0
            ddxsl=0; %ddxsl=0
            dxsl=0; %dxsl=0
        end
        if u(12)<90.5e-3-(2e-3*tan(phi))
            u(12)=90.5e-3-(2e-3*tan(phi));
            ddysd=0;
            dysd=0;
        end
    end
end

P2=[wg;dwg;dxsr;wsr;ddxsr;dwsr;dxsl;wsl;ddxsl;dwsl;dxsd;dysd;ddxsd;ddy
sd];

end
```

**Phase 3:**

```
function P3=phase3(t,u)
%Motion equations phase 3: Angular velocity synchronization
%Input variables:
u=u=[1)thetag,2)wg,3)xsr,4)thetasr,5)dxsr,6)wsr,7)xsl,8)thetasl,9)dxsl
,10)wsl,11)xsd,12)ysd,13)dxsd,14)dysd]'

%Rotating inertias [kg·m^2]
J1=0.17;
Jsr=4.0258e-3;
Jsl=1.4413e-2;
Jsd=5.4717e-4;
J5=6.1429e-2*2;

Rc=75e-3; %Mean cone radius [m]
Rsl=93.65e-3; %Mean effective radius on interlock gearing [m]
b=6.95e-3; %Half length of cone generatrix [m]
alphac=6*pi/180; %Cone angle [rad]
beta=60*pi/180; %Chamfer angle [rad]

cdrag1=0.02; %Oil viscous damping [kg·m^2/s]
cdrag2=0.03; %Oil viscous damping [kg·m^2/s]

S1=0.5; %From Stribeck's curve (number at the end of the mixed
friction)
S2=5; %From Stribeck's curve (number at the start of the mixed
friction)
musolid=0.09; %Friction coef. at the end of the mixed stage (Ref.
Paffoni et al., 2000)
muvis=0.02; %Friction coef. at the start of the mixed stage (Ref.
Paffoni et al., 2000)
mus=0.1; %Friction coef. between sleeve and synchro ring
dynvis=1.8e-5*839.4; %Dynamic viscosity [Pa·s] ATF at 60°C

Feff=35; %Load applied by the driver at the shift lever [N], Maximum
value allowed: 180-250 N
Feff_max=90; %Max effort applied by the driver [N]
eff=0.6; %Efficiency of the shift mechanism (normally <70%)
TR=7; %Transmission ratios of the shift mechanism (Normally varies
between 7:1 and 12:1)
Ffork0=Feff*eff*TR; %Load on the sleeve [N]
Ffork_max=Feff_max*eff*TR; %Max load on the sleeve [N]
Inc_Ffork=(Ffork_max-Ffork0)/0.2;

Ffork=Ffork0+Inc_Ffork*t;
Nc=Ffork/sin(alphac);

%------------------------------Equations-------------------------------
-----

q=1+1/3*(b/Rc)^2*(sin(alphac))^2;

%--------------------------Motion equations--------------------------
----
    %Change of variable:
%P3=zeros(14,1);
%P3=[1)wg,2)dwg,3)dxsr,4)wsr,5)ddxsr,6)dwsr,7)dxsl,8)wsl,9)ddxsl,10)dw
sl,11)dxsd,12)dysd,13)ddxsd,14)ddysd]'
```

```
wg=u(2); %wg
dxsr=u(5); %dxsr
wsr=u(6); %wsr

muc=musolid+((musolid-muvis)/(S2-S1)*S1)-(((musolid-muvis)/(S2-
S1))*(dynvis*Rc*(wsr-wg))/Ffork)*4*pi*Rc*b*sin(alphac); %Friction
coef. between cone surfaces
dwg=-(1/J1)*(muc*Nc*Rc*q+cdrag1*wg); %dwg

ddxsr=0; %ddxsr
dwsr=1/(Jsr+Jsl+Jsd+J5)*(muc*Nc*Rc*q-cdrag2*wsr); %dwsr
dwsl=dwsr; %dwsl=dwsr
dxsl=u(9); %dxsl
wsl=u(10); %wsl
ddxsl=0; %ddxsl
dxsd=u(13); %dxsd
dysd=u(14); %dysd
ddxsd=0; %ddxsd
ddysd=0; %ddysd

P3=[wg;dwg;dxsr;wsr;ddxsr;dwsr;dxsl;wsl;ddxsl;dwsl;dxsd;dysd;ddxsd;ddy
sd];

end
```

**Process (main function):**

```
%Synchronization process
function process_TOT

%-------------------------Solution phase 1-------------------------
----
u10=[0;4300*pi/30;17.25e-3;-
3*pi/180;0;3800*pi/30;0;0;0;3800*pi/30;0;90.5e-3;0;0]; %Initial
conditions of phase 1
t10=0; %Simulation starting time for phase 1
t1f=0.01; %Simulation final time for phase 1

options=odeset('Events',@events1,'Stats','on'); %Create an options
variable
[t1,u1]=ode45(@phase1,[t10 t1f],u10,options);

    function [value,isterminal,direction]=events1(t1,u1)
        value=u1(11)-1e-3; %Stops when u1(11)=1e-3
        isterminal=1; %Stop after the first event (=0 to get all the
events)
        direction=0; % No matter which direction (+ -> -  or - -> +)
    end

%-------------------------Solution phase 2-------------------------
----
msr=1.127;
np=3;
msd=0.166/np;
phi=45*pi/180;

u20=u1(end,:); %End conditions of phase 1 (initial conditions for
phase 2)
t20=t1(end); %Simulation starting time for phase 2

u20(13)=(msd*np*u1(end,13))/(msr+msd*np);
u20(5)=u20(13);
u20(9)=u20(13)+(abs(u1(end,14)/tan(phi)));

t2f=0.08; %Simulation final time for phase 2

options=odeset('Events',@events2,'Stats','on'); %Create an options
variable
[t2,u2]=ode45(@phase2,[t20 t2f],u20,options);

    function [value,isterminal,direction]=events2(t2,u2)
        value=u2(3)-(u1(end,3)+(5e-3-1e-6)); % Stops when
u2(3)=u20(3)+(5e-3-1e-6);
        isterminal=1; %Stop after the first event (=0 to get all the
events)
        direction=0; % No matter which direction (+ -> -  or - -> +)
    end

%-------------------------Solution phase 3-------------------------
----
u30=u2(end,:); %End conditions of phase 2 (initial conditions for
phase 3)
t30=t2(end); %Simulation starting time for phase 3
u30(5)=0; %Synchro ring does not move axially in phase 3
```

```
u30(9)=0; %Sleeve does not move axially in phase 3
u30(13)=0; %Strut detent does not move axially in phase 3
u30(14)=0; %Strut detent does not move radially
t3f=1; %Simulation final time for phase 3

options=odeset('Events',@events3,'Stats','on'); %Create an options
variable
[t3,u3]=ode45(@phase3,[t30 t3f],u30,options);

    function [value,isterminal,direction]=events3(t3,u3)
        value=u3(2)-u3(10); %Stops when angular velocities of gear and
sleeve are equal: u3(2)=u3(10)
        isterminal=1; %Stop after the first event (=0 to get all the
events)
        direction=0; % No matter which direction (+ -> -  or - -> +)
    end

t40=t3(end); %Simulation starting time for phase 4
%------------------------------Plots-----------------------------------
----
%   Angles
figure('numbertitle','off','name','theta_g,theta_sr,theta_sl')
subplot(3,1,1),plot(t1,u1(:,1)*180/pi,t2,u2(:,1)*180/pi,t3,u3(:,1)*180
/pi);
grid;
title('Angular displacement, body 1');
xlabel('Time [s]');
ylabel('\theta _{g} [deg]');

subplot(3,1,2),plot(t1,u1(:,4)*180/pi,t2,u2(:,4)*180/pi,t3,u3(:,4)*180
/pi);
grid;
title('Angular displacement, synchro ring');
xlabel('Time [s]');
ylabel('\theta_{sr} [deg]');

subplot(3,1,3),plot(t1,u1(:,8)*180/pi,t2,u2(:,8)*180/pi,t3,u3(:,8)*180
/pi);
grid;
title('Angular displacement, sleeve');
xlabel('Time [s]');
ylabel('\theta_{sl} [deg]');

%   Displacements
figure('numbertitle','off','name','x_sr,x_sl,x_sd,y_sd')
subplot(2,2,1),plot(t1,u1(:,3)*1000,t2,u2(:,3)*1000,t3,u3(:,3)*1000);
grid;
title('Axial displacement, synchro ring');
xlabel('Time [s]');
ylabel('x_{sr} [mm]');

subplot(2,2,2),plot(t1,u1(:,7)*1000,t2,u2(:,7)*1000,t3,u3(:,7)*1000);
grid;
title('Axial displacement, sleeve');
xlabel('Time [s]');
ylabel('x_{sl} [mm]');

subplot(2,2,3),plot(t1,u1(:,11)*1000,t2,u2(:,11)*1000,t3,u3(:,11)*1000
);
grid;
```

```
title('Axial displacement, strut detent');
xlabel('Time [s]');
ylabel('x_{sd} [mm]');

subplot(2,2,4),plot(t1,u1(:,12)*1000,t2,u2(:,12)*1000,t3,u3(:,12)*1000
);
grid;
title('Radial displacement, strut detent');
xlabel('Time [s]');
ylabel('y_{sd} [mm]');

%   Angular velocities
figure('numbertitle','off','name','w_g,w_sr,w_sl');
subplot(3,1,1),plot(t1,u1(:,2)*30/pi,t2,u2(:,2)*30/pi,t3,u3(:,2)*30/pi
);
grid;
title('Angular velocity, body 1');
xlabel('Time [s]');
ylabel('\omega_{g} [rpm]');

subplot(3,1,2),plot(t1,u1(:,6)*30/pi,t2,u2(:,6)*30/pi,t3,u3(:,6)*30/pi
);
grid;
title('Angular velocity, synchro ring');
xlabel('Time [s]');
ylabel('\omega_{sr} [rpm]');

subplot(3,1,3),plot(t1,u1(:,10)*30/pi,t2,u2(:,10)*30/pi,t3,u3(:,10)*30
/pi);
grid;
title('Angular velocity, sleeve');
xlabel('Time [s]');
ylabel('\omega_{sl} [rpm]');

figure('numbertitle','off','name','w_g,w_sl');
hold on
plot(t1,u1(:,2)*30/pi,t2,u2(:,2)*30/pi,t3,u3(:,2)*30/pi);
plot(t1,u1(:,10)*30/pi,'-.',t2,u2(:,10)*30/pi,'-
.',t3,u3(:,10)*30/pi,'-.');
grid;
title('Gear and sleeve angular velocities');
xlabel('Time [s]');
ylabel('\omega [rpm]');
legend('phase1','phase2','phase3');
hold off

%   Axial velocities
figure('numbertitle','off','name','dx_sr,dx_sl,dx_sd,dy_sd')
subplot(2,2,1),plot(t1,u1(:,5)*1000,t2,u2(:,5)*1000,t3,u3(:,5)*1000);
grid;
title('Axial velocity, synchro ring');
xlabel('Time [s]');
ylabel('dx_{sr} [mm/s]');

subplot(2,2,2),plot(t1,u1(:,9)*1000,t2,u2(:,9)*1000,t3,u3(:,9)*1000);
grid;
title('Axial velocity, sleeve');
xlabel('Time [s]');
ylabel('dx_{sl} [mm/s]');
```

```
subplot(2,2,3),plot(t1,u1(:,13)*1000,t2,u2(:,13)*1000,t3,u3(:,13)*1000
);
grid;
title('Axial velocity, strut detent');
xlabel('Time [s]');
ylabel('dx_{sd} [mm/s]');

subplot(2,2,4),plot(t1,u1(:,14)*1000,t2,u2(:,14)*1000,t3,u3(:,14)*1000
);
grid;
title('Radial velocity, strut detent');
xlabel('Time [s]');
ylabel('dy_{sd} [mm/s]');

Time=[t20 t30-t20 t40-t30]; %Duration of each phase separately
end
```